ADAMTS7 promotes smooth muscle foam cell expansion in atherosclerosis

Allen Chung[1], Lauren E. Fries[1], Hyun-Kyung Chang[1], Huize Pan[1, 2], Alexander C. Bashore[1, 3], Karissa Shuck[1], Caio V. Matias[1], Juliana Gomez Pardo[1], Jordan S. Kesner[1], Hanying Yan[4], Mingyao Li[4], Robert C. Bauer[1]*

[1]Cardiometabolic Genomics Program, Division of Cardiology, Department of Medicine, Columbia University, New York, NY, USA

[2]Present address: Division of Cardiovascular Medicine, Department of Medicine, Vanderbilt University Medical Center, Nashville, TN, USA

[3]Present address: Cardiovascular Research Institute, Icahn School of Medicine at Mount Sinai, New York, NY, USA

[4]Department of Biostatistics, Epidemiology and Informatics, University of Pennsylvania Perelman School of Medicine, Philadelphia, PA, USA

***Correspondence to**

Robert C. Bauer, Ph.D.

630 W. 168th Street, PS10-401,

New York, NY 10032, USA.

Telephone: +1-212-342-0952

E-mail: rcb36@columbia.edu

The authors have declared that no conflict of interest exists.

ABSTRACT

Human genetic studies have repeatedly associated *ADAMTS7* with atherosclerotic cardiovascular disease. Subsequent investigations in mice demonstrated that ADAMTS7 is proatherogenic and induced in response to vascular injury. However, the cell-specific mechanisms governing ADAMTS7 proatherogenicity remain unclear. To determine which vascular cell types express *ADAMTS7*, we interrogated single-cell RNA sequencing of human carotid atherosclerosis and found *ADAMTS7* expression in smooth muscle cells (SMCs), endothelial cells (ECs), and fibroblasts. We subsequently created SMC- and EC-specific *Adamts7* conditional knockout and transgenic mice. Conditional knockout of *Adamts7* in either cell type does not reduce atherosclerosis, whereas transgenic induction in either cell type increases atherosclerosis. In SMC transgenic mice, this increase coincides with an expansion of lipid-laden SMC foam cells and a decrease in fibrous cap formation. RNA-sequencing in *Adamts7* overexpressing SMCs revealed an upregulation of lipid genes typically assigned to macrophages. Mechanistically, ADAMTS7 increases SMC oxLDL uptake through CD36, whose expression is upregulated by PU.1. ATAC-seq and motif analysis revealed increased chromatin accessibility at AP-1 enriched regions, consistent with AP-1 dependent remodeling of PU.1-regulated lipid-handling loci. In summary, ADAMTS7 promotes atherosclerosis by driving SMC foam cell formation through an AP-1/PU.1/CD36 regulatory axis.

53 **INTRODUCTION**

54 Coronary artery disease (CAD) is the leading cause of death in the United States despite the widespread
55 availability of multiple highly effective lipid lowering therapies (1). Thus, there remains a need for novel,
56 non-lipid lowering therapeutic approaches for the treatment of CAD. Human genome-wide association
57 studies (GWAS) have proven an effective, unbiased approach to discovering novel genomic loci
58 associated with CAD, potentially uncovering therapeutic targets. GWAS have repeatedly identified the
59 15q25 locus as a region of interest for CAD (2-5). This locus harbors the gene A disintegrin and
60 metalloproteinase with thrombospondin motifs 7 (*ADAMTS7*), which encodes a secreted matrix
61 metalloproteinase previously implicated in osteoarthritis (6). After its identification by GWAS, subsequent
62 mouse studies demonstrated that ADAMTS7 is proatherogenic, as mice with whole-body *Adamts7*
63 knockout had reduced atherosclerosis (7). Notably, this reduction in atherosclerosis occurred without any
64 changes in plasma lipoprotein levels, suggesting that ADAMTS7 has a lipid-independent role in
65 atherogenesis (8). Further mouse models of *Adamts7* have confirmed this proatherogenicity while
66 demonstrating that ADAMTS7 catalytic activity is required for this effect (9, 10). Collectively, these
67 findings identify ADAMTS7 as an attractive lipid-independent therapeutic target for CAD, although the
68 molecular mechanisms linking ADAMTS7 to atherogenesis remain incompletely understood.

69

70 There has recently been an increased appreciation for the role of smooth muscle cells (SMCs) in
71 atherosclerosis (11). Although historically viewed primarily as contributors to fibrous cap formation,
72 single-cell RNA sequencing (scRNA-seq) studies in mice and humans have revealed that SMCs are
73 highly plastic and capable of undergoing phenotypic modulation, acquiring features of multiple cell types,
74 including macrophage-like characteristics (12, 13). Consistent with this plasticity, studies in the *Apoe*$^{-/-}$
75 model of atherosclerosis demonstrated that most lipid-laden aortic foam cells are not macrophages but
76 cells of SMC origin, highlighting that SMC foam cells may play a more significant role in atherogenesis
77 than previously understood (14). Mechanistic studies of ADAMTS7 have largely focused on its effects on
78 SMC function, as both *Adamts7* knockout and overexpression alter neointima formation following

79 vascular injury and modulate SMC migration in ex vivo assays (7, 15). As ADAMTS7 is a secreted
80 protein, it may influence multiple vascular cell types through both cell-autonomous and paracrine
81 mechanisms (16). *Adamts7* is not constitutively expressed in vascular cells, but rather, its expression is
82 induced in response to vascular injury and cytokine signaling (7, 9). Low basal expression of *Adamts7* in
83 vivo, together with its transient induction, has hindered efforts to identify the cell types that express
84 *Adamts7* and to define its function during atherosclerosis (7). Overall, ADAMTS7 has consistently been
85 linked to SMC function, yet the mechanistic basis by which this association promotes atherosclerosis
86 remains unknown (8).
87
88 In this study, we identified *ADAMTS7* expression across multiple human vascular cell types, including
89 SMCs and endothelial cells (ECs). We additionally generated several novel tissue-specific *Adamts7*
90 mouse models, enabling mechanistic interrogation of ADAMTS7 under conditions of sustained induction
91 or targeted deletion. Using these models, we demonstrate that *Adamts7* expression in either SMCs or
92 ECs is individually sufficient to increase atherosclerosis and promote SMC foam cell formation, whereas
93 deletion in either cell type alone does not significantly affect lesion burden. Mechanistically, we found that
94 ADAMTS7 alters the chromatin landscape of SMCs, inducing expression of the myeloid transcription
95 factor (TF) PU.1, increasing *Cd36* expression, and enhancing SMC oxidized low-density lipoprotein
96 (oxLDL) uptake. Together, these findings demonstrate that ADAMTS7 drives SMC foam cell expansion
97 and, ultimately, atherosclerosis.
98
99 **RESULTS**
100 ***ADAMTS7* is induced within multiple vascular cell types during lesion formation**
101 Prior literature indicates that *Adamts7* expression is induced within the vasculature and promotes SMC
102 migration while inhibiting re-endothelialization (7, 17). ADAMTS7 is secreted (18), and as such, the cell
103 type that responds to it does not necessarily have to produce it. Thus, to determine the cellular origins of
104 ADAMTS7, we interrogated the largest human atherosclerotic carotid artery scRNA-seq dataset

105 generated to date (19) and found that multiple vascular cell types express *ADAMTS7* in mature plaques.
106 The highest *ADAMTS7* expression was present in ECs, whereas SMCs, fibroblasts, and mast cells
107 displayed *ADAMTS7* expression at a lower level (Figure 1A). Interestingly, the highest level of *ADAMTS7*
108 expression occurred in ECs annotated as inflammatory (19), whereas fibrotic ECs did not display as high
109 a level of expression.
110
111 We next sought to confirm this observation in mouse models of atherosclerosis. Previous work in *Apoe*$^{-}$
112 $^{/-}$ mice has shown that *Adamts7* expression is induced after four weeks of western-type diet (WTD)
113 feeding but absent by terminal time points (7). To determine when *Adamts7* is expressed during
114 atherosclerosis, we performed RNAscope within the brachiocephalic artery (BCA) of hyperlipidemic Low-
115 Density Lipoprotein Receptor knockout (*Ldlr*^{KO}) mice at four, six, and nine weeks of WTD. *Adamts7*
116 expression appears during early atheroma formation and is especially prominent at nine weeks when
117 established lesions are present (Figure 1B). Across multiple experiments, *Adamts7* expression was
118 localized to the developing atherosclerotic neointima and to multiple other locations in the BCA,
119 consistent with its expression in SMCs and other cells (Figure 1, B-D). To confirm EC expression as seen
120 in the human scRNA-seq data, we performed RNAscope in the BCA of *Ldlr*^{KO} mice after seven and ten
121 weeks of WTD (Figure 1, C and D). At the early lesion time point of seven weeks, we detected
122 colocalization of the *Adamts7* transcript with *Pecam1*, an EC marker, while at the ten-week time point,
123 we observed *Adamts7* expression in both ECs and non-ECs. These data support the notion that multiple
124 vascular cell types produce ADAMTS7 during atherosclerosis in mice and humans.
125
126 **SMC or EC specific knockout of *Adamts7* does not reduce atherosclerosis.**
127 Given *Adamts7* expression in multiple vascular cell types, we next asked if the knockout of *Adamts7* in
128 any single vascular cell type could reduce atherosclerosis. We generated a conditional knockout model
129 of *Adamts7* where exons five and six are floxed (Supplemental Figure 1A). Given the strong
130 prior literature on ADAMTS7 regulation of SMC function, we crossed this mouse to the *Myh11*-CreER^{T2}

131 and *Ldlr*^{KO} to generate a hyperlipidemic SMC conditional knockout of *Adamts7* (*Adamts7*$^{fl/fl}$; *Ldlr*^{KO};
132 *Myh11*-CreER^{T2}, referred to as *Adamts7*^{SMCKO} *Ldlr*^{KO}) and subsequently induced knockout through
133 intraperitoneal tamoxifen injections (Figure 2A). Although *Adamts7* expression is typically low in uninjured
134 vessels, SMC explants from *Adamts7*^{SMCKO} *Ldlr*^{KO} mice exhibited an approximately 50% reduction in
135 *Adamts7* expression compared with wild-type controls *Adamts7*^{SMCWT} *Ldlr*^{KO} (Supplemental Figure 1B).
136 Following 16 weeks of WTD feeding, we observed no changes in body weight or total cholesterol
137 (Supplemental Figure 1, D and E). Surprisingly, *Adamts7*^{SMCKO} *Ldlr*^{KO} did not alter the lesion area in either
138 en face Oil Red O (ORO) analysis (Figure 2B) or aortic root lesion area (Figure 2C). Because *ADAMTS7*
139 expression is also prominent in ECs based on human scRNA-seq data (Figure 1A), we next generated
140 an *Adamts7* EC-specific conditional knockout by crossing the hyperlipidemic conditional knockout mouse
141 to the *Cdh5*-CreER^{T2} (*Adamts7*$^{fl/fl}$; *Ldlr*^{KO}; *Cdh5*-CreER^{T2}, referred to as *Adamts7*^{ECKO} *Ldlr*^{KO}). To confirm
142 EC-specific knockout, we isolated CD31^{+} ECs from aortas and observed markedly reduced *Adamts7*
143 expression in the CD31^{+} fraction from *Adamts7*^{ECKO} *Ldlr*^{KO} mice compared with wild-types (*Adamts7*^{ECWT}
144 *Ldlr*^{KO}), whereas no difference was observed in the CD31^{-} (non-EC) fraction (Supplemental Figure 1C).
145 After 16 weeks of WTD feeding, we assessed atherosclerosis in *Adamts7*^{ECKO} *Ldlr*^{KO} compared to
146 *Adamts7*^{ECWT} *Ldlr*^{KO} (Figure 2D). Again, we observed no changes in body weight or total cholesterol levels
147 (Supplemental Figure 1, F and G). Similar to *Adamts7*^{SMCKO} *Ldlr*^{KO} mice, EC knockout of *Adamts7* also
148 did not demonstrate any changes in the atherosclerotic burden (Figure 2, E and F). These data strongly
149 suggest that individual knockout of *Adamts7* in ECs or SMCs alone is not adequate to alter atherogenesis
150 in mice.
151

152 **Transgenic overexpression of *Adamts7* in mouse SMCs or ECs exacerbates atherosclerosis.**
153 Given that knockout of *Adamts7* in either SMCs or ECs alone does not appear to reduce atherogenesis
154 in our model, we next asked whether sustained induction of *Adamts7* expression in a single cell type can
155 increase atherogenesis. As *ADAMTS7* is induced in multiple vascular cell types in human atherosclerosis
156 (Figure 1A), we generated a transgenic mouse model with conditional *Adamts7* overexpression to mimic

157 its induction and promote its function in multiple cell types. We inserted murine *Adamts7* into the Rosa26
158 locus with a lox-stop-lox (LSL) cassette preceding the gene, allowing for tissue type-specific
159 overexpression of *Adamts7*. The transgenic overexpression model was subsequently bred to the *Ldlr*^{KO}
160 background as well as to either the *Myh11*-CreER^{T2} (*Adamts7*^{SMCTG}) or the *Cdh5*-CreER^{T2} (*Adamts7*^{ECTG})
161 to allow for SMC (Figure 3A) or EC (Figure 3G) specific overexpression of *Adamts7,* respectively. We
162 verified *Adamts7* overexpression in the SMC transgenic model via qPCR (Supplemental Figure 2A) and
163 western blot (Supplemental Figure 2B) from isolated aortic RNA and protein. We note that *Adamts7*^{SMCTG}
164 *Ldlr*^{KO} exhibited a large-fold change in *Adamts7* RNA, but this is partly due to the near complete absence
165 of baseline expression of *Adamts7*. Primary SMC explants from *Adamts7*^{SMCTG} displayed increased
166 migration (Supplemental Figure 2C), consistent with prior findings (7). Validation of *Adamts7*^{ECTG} was
167 achieved by examining *Adamts7* expression in isolated CD31^{+} vascular ECs as well as mouse lung ECs
168 (Supplemental Figure 2D); *Adamts7* expression was elevated in ECs, whereas CD31^{-} cells showed no
169 difference in *Adamts7* expression.
170
171 To investigate the role of sustained cellular *Adamts7* in atherosclerosis development, *Adamts7*
172 overexpression was induced in all animal models via tamoxifen injection, and mice were fed a WTD for
173 16 weeks. There were no plasma cholesterol or body weight changes in any animal models
174 (Supplemental Figure 3, E-H). *Adamts7*^{SMCTG} *Ldlr*^{KO} mice had a stark 3.5-fold increase in atherosclerosis
175 as shown by en face ORO staining as compared to control *Adamts7*^{SMCCTL} *Ldlr*^{KO} mice (Figure 3B), but
176 no change in the aortic root lesion area as assessed by H&E staining (Figure 3C), consistent with findings
177 in other *Adamts7* mouse models (9). Given the dramatic increase in aortic atherosclerosis, we asked
178 whether shorter durations of WTD feeding would confer an atherosclerosis phenotype. Indeed, we found
179 increased atherosclerosis at three, six, and nine weeks of WTD feeding (Supplemental Figure 3A).
180
181 During atherosclerosis, SMCs play an essential role in plaque stabilization (20). As such, we further
182 characterized the aortic root plaque morphology in *Adamts7*^{SMCTG} *Ldlr*^{KO} mice. We found no changes in

183 necrotic core area (Figure 3D) or macrophage content via MAC2 staining (Figure 3E). However,
184 *Adamts7*^{SMCTG} *Ldlr*^{KO} lesions had reduced SMC content as determined by α-SMA staining (Figure 3E),
185 especially in the fibrous cap region. The reduction in α-SMA also coincided with a 48% reduction in fibrous
186 cap thickness as assessed through picrosirius red staining (Figure 3F). The lack of change in MAC2
187 staining and the reduction in cap thickness indicate that increased ADAMTS7 reduces indices associated
188 with human plaque stability in these mouse models. Finally, in tandem, we performed a similar
189 atherosclerosis study on the *Adamts7*^{ECTG} *Ldlr*^{KO} mice and observed a 1.5-fold increase in aortic
190 atherosclerosis in *Adamts7*^{ECTG} *Ldlr*^{KO} mice as compared to controls (Figure 3H). We also observed the
191 same lack of changes in aortic root lesion area between groups (Figure 3I).
192
193 ***Adamts7* promotes SMC foam cell formation.**
194 The significant increase in ORO staining of the en face aorta indicates an increased accumulation of
195 neutral lipids within vascular cells, presumably due to an expansion in foam cell formation. Thus, we next
196 sought to assess aortic foam cell content in our *Adamts7* transgenic mice using a neutral lipid dye,
197 LipidTOX. After excluding debris, doublets, and dead cells (Supplemental Figure 4A), we observed that
198 the *Adamts7*^{SMCTG} *Ldlr*^{KO} had a threefold increase in foam cell content, mirroring the rise in aortic
199 atherosclerosis (Figure 4A). Notably, over 80% of these foam cells lacked CD11B and CD64, indicating
200 that non-leukocytes are accumulating lipids and becoming foamy (Figure 4B) (21). Given that increased
201 ORO staining of the aorta was evident even at early time points, we next examined foam cell composition
202 after 3 weeks of WTD. Despite the short feeding period, *Adamts7*^{SMCTG} *Ldlr*^{KO} mice already exhibited a
203 significant increase in foam cell formation, driven primarily by an expansion of SMC-derived foam cells
204 as identified by CD200 expression (Supplemental Figure 3B).
205
206 To further confirm that the increase in foam cells was predominantly of SMC origin, the *Adamts7*^{SMCCTL}
207 *Ldlr*^{KO} and *Adamts7*^{SMCTG} *Ldlr*^{KO} mouse model was subsequently bred to an LSL-ZsGreen reporter
208 (*Adamts7*^{SMCCTL} *Ldlr*^{KO} ZsGreen^{SMC+} and *Adamts7*^{SMCTG} *Ldlr*^{KO} ZsGreen^{SMC+}) to allow for the lineage

209 tracing of SMCs and their derived cells (12). Efficient ZsGreen labeling of SMCs was achieved through
210 microscopy (Figure 4C). After 12 weeks of WTD feeding, ZsGreen status and concurrent staining with
211 CD45, revealed that over 65% of lipid-laden foam cells were ZsGreen^{+} and CD45^{-} (Supplemental Figure
212 4B), indicating again that *Adamts7* was predominately increasing SMC foam cell formation (Figure 4D).
213 We repeated the foam cell analysis within *Adamts7*^{ECCTL} *Ldlr*^{KO} and *Adamts7*^{ECTG} *Ldlr*^{KO} and observed
214 that the *Adamts7*^{ECTG} *Ldlr*^{KO} mice contained an increase in foam cell content as well (Figure 4E). Further
215 assessment of these foam cells within the aorta revealed that the majority were CD45^{-} and CD31^{-} while
216 being CD200^{+} (21), indicating again that SMCs are also becoming foamy in this model (Figure 4F).
217
218 To test if ADAMTS7 promotes SMC foam cell formation by enhancing lipid uptake, we generated primary
219 SMC explants from the *Adamts7*^{SMCCTL} and *Adamts7*^{SMCTG} mice with wild-type *Ldlr* and treated them with
220 fluorescently labeled oxLDL (DiI-oxLDL). We chose oxLDL as it is a pathophysiologically relevant
221 modified lipoprotein that accumulates within atherosclerotic lesions (22). *Adamts7*^{SMCTG} primary SMCs
222 showed a 38% increase in DiI-oxLDL uptake compared to *Adamts7*^{SMCCTL} as measured by median
223 fluorescence intensity (MFI) (Figure 4G). Both the proportion of DiI-oxLDL positive cells and the intensity
224 of staining per cell were elevated in the *Adamts7*^{SMCTG} group. To further validate the role of *Adamts7* in
225 SMC lipid uptake, we examined primary SMCs isolated from our previously described global *Adamts7*
226 knockout mice (7). Following TNFα stimulation for 72 hours to induce *Adamts7* expression, the SMCs
227 were loaded with DiI-oxLDL. Knockout of *Adamts7* reduced the percentage of cells accumulating lipids
228 and the amount of lipid uptake (Figure 4H), complementing the transgenic phenotype.
229
230 ***Adamts7* leads to an increase in lipid uptake gene expression in SMCs.**
231 To identify how ADAMTS7 mediates an increase in SMC lipid uptake, we performed bulk RNA-seq on
232 SMCs explanted from *Adamts7*^{SMCCTL} and *Adamts7*^{SMCTG} mouse aortas ten days after transgene induction
233 (Figure 5A). These cells were from mice with wild-type *Ldlr* expression and fed a chow diet, ensuring that
234 any changes in gene expression are due specifically to increased *Adamts7* expression. Differential gene

235 expression analysis revealed that *Adamts7*^{SMCTG} cells had increased expression of lipid uptake genes
236 typically associated with macrophages, including *Cd36, Fabp5*, and *Trem2,* as well as the macrophage-
237 associated marker *Adgre1*. Importantly, this represents a transcriptional elevation; these cells are not
238 bona fide macrophages. These findings were validated in vivo by qRT-PCR of whole aorta RNA from
239 *Adamts7*^{SMCTG} mice (Figure 5B). While the increase in macrophage-like gene expression indicates SMC
240 phenotypic modulation, we did not observe decreases in canonical SMC contractile markers, either by
241 RNA-seq or by qRT-PCR (Supplemental Figure 5A), even with oxLDL treatment (Supplemental Figure
242 5B). Similarly, the expression of *Klf4*, a marker typically associated with modulated SMCs remained
243 unchanged even with oxLDL treatment (13). Ingenuity Pathway Analysis (IPA) on the differentially
244 expressed gene set identified pathways enriched within the *Adamts7*^{SMCTG} SMCs typically ascribed to
245 macrophages, such as phagosome formation and immune signaling (Figure 5C). As one of the hallmark
246 functions of macrophages during atherosclerosis is perpetuating inflammation, we asked whether our
247 *Adamts7*^{SMCTG} SMCs were more inflammatory. Cytokine analysis of conditioned media revealed no
248 differences in IL1β, IL6, or TNFα secretion (Supplemental Figure 5C). These findings indicate that
249 *Adamts7*^{SMCTG} SMCs are not inflammatory and any atherosclerosis phenotype is likely independent of
250 canonical inflammatory pathways. Collectively, the RNA-seq and qRT-PCR data indicate that
251 *Adamts7*^{SMCTG} SMCs acquire a gene signature typically associated with macrophages, with an
252 enrichment of phagocytic and lipid-uptake genes, consistent with prior reports that modulated SMCs can
253 upregulate macrophage processes (12, 23).
254
255 **Knockdown of *Cd36* ameliorates enhanced oxLDL uptake conferred by *Adamts7*.**
256 Given the known role of CD36 as a receptor for oxLDL (24), we next investigated whether CD36 mediates
257 the increased lipid uptake observed in *Adamts7*^{SMCTG} cells. Flow cytometric analysis was used on
258 *Adamts7*^{SMCTG} *Ldlr*^{KO} ZsGreen^{SMC+} aortas after 12 weeks of WTD feeding to examine CD36 levels in vivo.
259 ZsGreen^{+} cells from *Adamts7*^{SMCTG} *Ldlr*^{KO} ZsGreen^{SMC+} mice had a 40% increase in cells
260 expressing *Cd36* and a 2.3-fold increase in MFI of CD36 signal (Figure 5D), consistent with the in vitro

261 increase in CD36 expression in *Adamts7*^{SMCTG} cells. To determine whether CD36 is functionally required
262 for ADAMTS7-induced lipid uptake, we performed siRNA-mediated knockdown of *Cd36* in primary SMCs
263 isolated from *Adamts7*^{SMCCTL} and *Adamts7*^{SMCTG} mice. siRNA-mediated knockdown of *Cd36* in primary
264 SMCs from *Adamts7*^{SMCTG} mice reduced *Cd36* expression to that of Non-Targeting Control (NTC) treated
265 *Adamts7*^{SMCCTL} cells (Figure 6A). Consistent with this, siCd36 treatment normalized oxLDL uptake in
266 *Adamts7*^{SMCTG} cells to levels comparable to NTC-treated controls (Figure 6B). Together, these data
267 demonstrate that ADAMTS7 promotes SMC lipid uptake through upregulation of *Cd36*, identifying CD36
268 as a key mediator of the enhanced oxLDL uptake and foam cell formation driven by ADAMTS7 during
269 atherogenesis.
270
271 **Knockdown of *Spi1* in *Adamts7* overexpressing SMCs attenuates the expression of macrophage-**
272 **like and lipid-uptake genes**.
273 We next used IPA to identify upstream transcriptional regulators that could mediate the observed
274 differential gene expression (Table 1) in *Adamts7*^{SMCTG} cells. The top predicted activated TF was *Spi1,*
275 which encodes the protein PU.1. *Spi1* itself also exhibited a 3.16-fold increase in expression in
276 *Adamts7*^{SMCTG} cells. To test whether PU.1 is required for the *Adamts7*-mediated increase in lipid uptake
277 genes, we used siRNA to achieve a 66% knockdown of *Spi1* in primary SMCs. Knockdown of *Spi1*
278 abrogated the increases in gene expression of *Cd36, Fabp5*, *Trem2, Adgre1*, and *Cd68* (Figure 6C). We
279 also performed siRNA knockdown of other predicted master regulator TFs identified by IPA and found
280 that knockdown of *Cebpa*, *Smarca4*, *Bhlhe40*, and *Klf6* did not ameliorate the increases in lipid uptake
281 gene expression (Supplemental Figure 6). DiI-oxLDL loading of primary *Adamts7*^{SMCTG} SMCs with *Spi1*
282 knockdown demonstrated that loss of *Spi1* attenuated the increased oxLDL uptake in *Adamts7*^{SMCTG} cells
283 while having no effect in *Adamts7*^{SMCCTL} primary SMCs (Figure 6D). This finding suggests that increased
284 *Spi1* levels resulting from *Adamts7* expression are responsible for the increased oxLDL uptake observed
285 in *Adamts7*^{SMCTG} SMCs. Finally, we examined the level of *SPI1* expression within our human single-cell
286 data and found clear *SPI1* expression in the modulated SMC populations (Figure 6E), mirroring our

287 observations in mice and suggesting that *SPI1* may contribute similarly to SMC phenotypic modulation
288 in humans. Within these human SMCs, phenotypic modulation was also accompanied by increased
289 expression of lipid-handling genes *CD36* (19), *FABP5,* and *TREM2*, as well as the macrophage marker
290 *ADGRE1* (Supplemental Figure 7).
291
292 **ADAMTS7 promotes an AP-1-dependent chromatin remodeling program in SMCs**
293 RNA-seq analysis revealed widespread transcriptional reprogramming in *Adamts7*^{SMCTG} SMCs (Figure
294 5), leading to increased oxLDL uptake. Given that ADAMTS7 is a secreted extracellular protein, these
295 changes must be driven by outside-in signaling that alters TF activity. To identify changes in TF activity,
296 we performed ATAC-seq on primary SMCs explanted from *Adamts7*^{SMCCTL} and *Adamts7*^{SMCTG} mice to
297 map regions with altered chromatin accessibility. Differential ATAC-seq peak analysis revealed that
298 *Adamts7* overexpression broadly remodels the chromatin landscape in SMCs, with 47,452 peaks (19.5%
299 of all ATAC peaks) showing differential accessibility between groups (Figure 7A). TF binding motif
300 analysis in the differential peaks identified enrichment of binding sites for FOS and JUN, members of the
301 AP-1 TF complex (Figure 7B). Integration of ATAC-seq with RNA-seq data (Figure 5) further
302 demonstrated that 85.8% of genes differentially expressed in *Adamts7*^{SMCTG} SMCs were associated with
303 a nearby differential ATAC peak (±100 kb from the transcription start site), indicating a close coupling
304 between chromatin accessibility and transcriptional reprogramming by ADAMTS7 (Figure 7C).
305
306 We next focused on the *Spi1* genomic locus in greater detail, chromatin accessibility increased markedly
307 within ±200 kb of the *Spi1* transcriptional start site (Supplemental Figure 8). Notably, a region of
308 differential accessibility within a *Spi1* intron overlaps both a predicted cis-regulatory element and AP-1
309 binding site, consistent with AP-1-dependent regulation of *Spi1* transcription in *Adamts7*^{SMCTG} SMCs
310 (Figure 7D). AP-1 transcriptional activity is canonically regulated by MAPK/ERK-dependent
311 phosphorylation of FOS and JUN, which enhances their DNA-binding and transactivation potential (25).
312 Consistent with this model, *Adamts7*^{SMCTG} SMCs displayed increased proliferation, a hallmark of

313 MAPK/ERK pathway activation, while SMCs isolated from global *Adamts7* knockout mice exhibited
314 slower proliferation, confirming that ADAMTS7 contributes to SMC proliferative capacity (Figure 7E). We
315 next tested whether inhibiting MAPK/ERK signaling could block ADAMTS7-induced phenotypes.
316 Treatment with Ulixertinib, a selective ERK1/2 inhibitor, significantly suppressed *Spi1* expression (Figure
317 7F), reduced the induction of *Cd36* and *Trem2*, and blunted oxLDL lipid accumulation (Figure 7G).
318 Together, these results are consistent with a model where ADAMTS7 promotes AP-1 activity, which in
319 turn upregulates *Spi1* and downstream lipid-handling genes, driving both transcriptional and phenotypic
320 reprogramming of SMCs.
321
322 Given that ADAMTS7 is a matrix metalloproteinase, we next investigated whether previously identified
323 ADAMTS7 extracellular matrix (ECM) substrates (THBS1, COMP, LTBP4, and TIMP1) mediate the
324 observed increases in lipid handling gene expression in *Adamts7*^{SMCTG} SMCs. To test this, we performed
325 siRNA knockdowns of putative substrates in primary SMCs from *Adamts7*^{SMCCTL} and *Adamts7*^{SMCTG} mice
326 (Supplemental Figure 9A). Among these, *Thbs1* knockdown most strongly attenuated the ADAMTS7-
327 induced upregulation of *Cd36, Spi1*, and *Trem2*, while *Fabp5* expression remained unaffected. Although
328 not fully restoring gene expression to baseline, this partial rescue indicates that *Thbs1* contributes in part
329 to ADAMTS7-dependent gene activation. In contrast, *Comp* silencing modestly reduced the expression
330 of select lipid-related genes with minor to no effects on *Cd36*, and knockdown of *Ltbp4* or *Timp1* produced
331 minimal effects. Finally, we assessed THBS1 and COMP protein levels by western blot of whole aortic
332 lysates following WTD feeding. This analysis revealed the presence of cleaved THBS1 fragments in
333 *Adamts7*^{SMCTG} lysates with no reduction in total THBS1 protein, whereas total COMP protein levels were
334 noticeably reduced (Supplemental Figure 9B). Collectively, these results demonstrate that ADAMTS7
335 promotes PU.1–dependent lipid uptake and transcriptional reprogramming in SMCs through a
336 combination of ECM substrate–mediated signaling and AP-1 dependent chromatin remodeling.
337
338

339 **DISCUSSION**

340 GWAS have revealed over 300 genomic regions associated with CAD (2, 26). Yet, functional studies
341 elucidating the precise mechanisms by which these loci influence disease are still limited, hampering the
342 clinical translation of these genetic findings. In 2011, our group and others reported *ADAMTS7* as a
343 GWAS gene for CAD (4). Subsequent GWAS studies have replicated this signal multiple times and
344 across different ethnic groups (2, 26), highlighting the importance of ADAMTS7 in CAD pathogenesis.
345 Experimental studies in mice demonstrated that ADAMTS7 is proatherogenic and that its atherogenicity
346 is conferred from its catalytic function (7, 9). Despite the sizable body of prior work on ADAMTS7, we still
347 do not understand how ADAMTS7 participates in atherogenesis. Additionally, there have not been any
348 cell-specific in vivo ADAMTS7 studies prior to this one, leaving the question of which vascular cell type(s)
349 is critical for ADAMTS7 function. Here, we identified prominent expression of ADAMTS7 in human and
350 mouse stromal and ECs and developed multiple novel mouse models in which *Adamts7* can be
351 genetically overexpressed or conditionally knocked out in a cell-specific manner. Through these models,
352 we demonstrate that both SMC- and EC-derived expression of *Adamts7* is proatherogenic, while
353 knockout of *Adamts7* in either cell type alone is not sufficient to alter atherogenesis. These findings
354 suggest that ADAMTS7 exerts redundant proatherogenic effects across multiple cell types through a
355 shared mechanism in which it promotes SMC foam cell formation by enhancing oxLDL uptake via
356 upregulation of *Spi1* and its downstream target *Cd36*.

357

358 *Adamts7* has very low overall expression across all murine vascular cell types in the basal state, and its
359 expression is induced in response to vascular injury such as endothelial denudation or prolonged
360 hyperlipidemia (7, 15). In primary mouse aortic SMCs, *Adamts7* induction is required to confer a
361 detectable migration phenotype (7), confirming that this induction is critical for ADAMTS7 function. At
362 terminal time points in mouse atherosclerosis studies, ADAMTS7 is again undetectable in plaques (7, 9),
363 suggesting that *Adamts7* induction is transient and ADAMTS7 is mechanistically active in mice during
364 plaque maturation. The transient induction of *Adamts7* has made studying its exact function in vascular

365 cells difficult. The novel *Adamts7* mouse models presented here overcome this limitation, demonstrating
366 that sustained *Adamts7* expression in either SMCs or ECs is sufficient to drive atherosclerosis
367 progression.
368
369 While neither *Adamts7*^{SMCKO} *Ldlr*^{KO} nor *Adamts7*^{ECKO} *Ldlr*^{KO} affected atherosclerosis, prior research on
370 whole-body knockout models indicates that *Adamts7* is pro-atherogenic. These prior published studies
371 include three unique models of whole-body *Adamts7* inactivation. Two models employed genetic
372 perturbation to inactivate ADAMTS7 by either exon deletion or mutation of the ADAMTS7 catalytic site
373 (7, 9), while the third approach was to vaccinate against ADAMTS7 (10). While prior findings clearly
374 demonstrate that *Adamts7* is expressed in cultured SMCs (7, 9, 15, 27), our RNAscope studies of
375 *Adamts7* expression revealed its induction in multiple vascular cell types during murine atherosclerosis,
376 yet only a small subset of vascular cells express *Adamts7* at any given time. Although we cannot exclude
377 the existence of a yet unidentified dominant producer cell type, the reproducible multicellular distribution
378 across independent datasets (19, 28) supports the view that *Adamts7* is broadly expressed and that its
379 proatherogenic effects likely arise through cooperative or redundant mechanisms among vascular cells.
380 Consistent with this, our data suggest that loss of *Adamts7* in a single cell type is insufficient to blunt
381 atherogenesis, while broad inactivation across multiple compartments as in whole-body knockout
382 reduces lesion burden (7, 9). Determining which combination of cell type–specific ADAMTS7 expression
383 is required to drive atherosclerosis will necessitate future double-knockout models employing multiple
384 Cre drivers.
385
386 Exactly how these findings translate to human atherosclerosis is another open question. Our analysis of
387 the most extensive carotid plaque single-cell data set to date highlights that ECs and SMCs both express
388 *ADAMTS7*, consistent with our murine findings and supporting the concept of multicellular expression in
389 advanced disease. This scRNA-seq data also shows that mast cells and fibroblasts have detectable
390 *ADAMTS7* expression, highlighting these cell types for further ADAMTS7 studies. Notably, the scRNA-

391 seq data comes from mature atherosclerotic plaques, while our mouse data suggests the window for
392 ADAMTS7 activity is earlier in plaque progression. Thus, whether this human expression pattern reflects
393 relevant ADAMTS7 activity remains to be determined. Moreover, the therapeutic potential of targeting
394 *ADAMTS7* in established lesions is unknown. Nonetheless, the human data indicate that ADAMTS7 is
395 active in multiple vascular cell types, and our mouse data shows that sustained ADAMTS7 activity in
396 individual cell types can drive atherogenesis. From a clinical perspective, much of the mechanistic
397 understanding of ADAMTS7 function in atherosclerosis has been derived from murine models. Future
398 studies examining functionally relevant *ADAMTS7* genetic variation, including the previously reported
399 S214P common variant (27), as well as yet unidentified loss-of-function variants that impair catalytic
400 activity, may help bridge mechanistic insights such as those described here with human disease
401 pathology.
402
403 Our SMC-specific and EC-specific *Adamts7* overexpression mouse models have increased
404 atherosclerotic burden and aortic foam cell formation, and these foam cells are SMC-derived. Although
405 macrophages have historically been thought to be the source of foam cells in atherosclerotic lesions, it
406 is increasingly appreciated that SMCs constitute most foam cells in atherosclerosis (14). Elegant fate
407 mapping and integrative genomic studies have revealed that SMCs can transition into diverse phenotypic
408 states, including inflammatory, fibroblast-like, and progenitor-like cells, through distinct transcriptional
409 programs regulated by TFs such as KLF4, OCT4, TCF21, and retinoid signaling (11). Our findings raise
410 the possibility that PU.1 is another TF directing SMCs specifically toward the foam cell fate. Consistent
411 with this, when *Adamts7* is induced in the vasculature, SMCs increase their expression of genes involved
412 in lipid uptake, inflammation, and phagocytosis, a gene expression profile reminiscent of a macrophage.
413 As recent studies have definitively shown that SMCs do not contribute to the pool of mature macrophages
414 in atherosclerosis (29), we posit that these *Adamts7*^{SMCTG} SMCs are modulated SMCs with increased
415 lipid uptake capacity and foam cell features. While the specific role of SMC foam cells in atherosclerosis
416 remains unclear, it has been reported that SMC foam cells and true macrophages differ in their

417 intracellular lipid metabolism (30, 31). Lipid-laden, foamy macrophages tend to be less inflammatory (32),
418 and by becoming foamy, these macrophages may no longer contribute to the inflammatory cycle
419 associated with atherosclerosis, raising the possibility that foamy macrophages are beneficial in
420 atherosclerosis. Conversely, we observed reduced fibrous cap thickness with *Adamts7* overexpression.
421 As one well-described role of SMCs is forming the fibrous cap, it is possible that foamy SMCs cannot
422 stabilize lesions, raising an intriguing possibility that macrophage foam cells are beneficial, whereas SMC
423 foam cells are detrimental. In Sharifi et al., the authors showed that ADAMTS7 degrades TIMP1,
424 increasing MMP2 and MMP9 activity (33). Consistent with that model, ADAMTS7 whole-body knockout
425 increased collagen content and plaque stabilization, and *ADAMTS7* expression was found to be higher
426 in caps of unstable human carotid plaques (33). These prior observations and those presented here
427 support the adverse role of ADAMTS7 in plaque stability and suggest multiple mechanistic explanations
428 for ADAMTS7-mediated plaque instability.
429
430 Mechanistically, we chose to pursue the function of SMC *Adamts7* given the large body of preexisting
431 data on *Adamts7* modulation of SMC function. We find that constitutive *Adamts7* SMC expression
432 markedly alters lipid uptake gene programs, resulting in enhanced oxLDL accumulation. Among these
433 lipid uptake genes, one of the most significantly upregulated genes was *Cd36*. CD36 is a well-described
434 receptor for oxLDL, and our studies demonstrate that CD36 is mainly responsible for the SMC foam cell
435 phenotype in *Adamts7*^{SMCTG} mice (24). In addition, upstream regulator analysis of primary SMCs identified
436 *Spi1* as a potential mediator of expression changes (34), and knockdown of *Spi1* in *Adamts7*^{SMCTG} SMCs
437 ameliorated the increase in lipid-handling gene expression and macrophage markers. *Spi1*, which
438 encodes the TF PU.1, is well recognized as a critical mediator of hematopoietic lineage commitment.
439 These observations suggest that PU.1 may also be a crucial factor in driving the in vivo production of
440 foamy SMCs. Thus, future cell-specific studies of SMC PU.1 may help reveal disease-relevant
441 consequences of foamy SMCs.
442

443 Using ATAC-seq, we observed that ADAMTS7 enhances chromatin accessibility and activates AP-1–
444 dependent transcription. AP-1 activity is regulated by MAPK signaling via ERK1/2, and pharmacologic
445 inhibition of ERK1/2 reduced ADAMTS7-induced expression of lipid-handling genes. These findings
446 support a model in which extracellular ADAMTS7 activates MAPK-ERK1/2 signaling, modulating AP-1
447 activity and altering SMC gene expression profiles. Importantly, this suggests that ADAMTS7-mediated
448 cleavage of an extracellular substrate triggers MAPK signaling cascades. ADAMTS7 substrates have
449 been proposed in prior studies (8, 33, 35, 36), but none have been tested in the context of SMC foam
450 cell formation. To explore this, we examined several previously proposed substrates and found that
451 *Thbs1* knockdown partially attenuated ADAMTS7-associated lipid gene expression. Western blot
452 analysis of aortic lysates revealed cleaved THBS1 fragments without a reduction in total THBS1 protein,
453 while COMP levels were modestly reduced, suggesting differential substrate processing in vivo. Notably,
454 *Comp* silencing also suppressed *Spi1* expression, raising the possibility that COMP may contribute to
455 ADAMTS7-mediated oxLDL uptake. Together, these findings support a model in which ADAMTS7-
456 dependent substrate processing, potentially involving both THBS1 and COMP, contributes to
457 downstream signaling. The identification of ADAMTS7 cleavage substrates remains an active area of
458 investigation. Although THBS1 and COMP have been previously reported as ADAMTS7 substrates (17,
459 37), not all studies have reproduced these findings (35), and the relative contribution of these substrates
460 remains undefined. Definitive evaluation of these substrates is necessary, as identifying biologically
461 meaningful cleavage products may reveal functional therapeutic biomarkers and inform the development
462 of targeted ADAMTS7-directed therapies.
463
464 In conclusion, our study establishes that ADAMTS7 promotes SMC foam cell formation and
465 atherosclerosis through PU.1 and CD36 and that its expression is not confined to a single vascular cell
466 type. By integrating human single-cell data with new cell-specific genetic models, we show that
467 ADAMTS7 is distributed across diverse vascular populations and that its sustained activation, whether
468 from SMCs or ECs, drives disease progression. These findings reveal a unifying mechanism linking

469 human GWAS data with cellular pathophysiology, reinforcing ADAMTS7 inhibition as a potential
470 therapeutic target for atherosclerotic cardiovascular disease.
471
472
473
474
475
476
477
478
479
480
481
482
483
484
485
486
487
488
489
490
491
492
493
494

495 **METHODS**

496 **Sex as a biological variable**

497 Our human data contained both male and female samples. SMC mouse studies were limited to male
498 mice due to the integration of the *Myh11*-CreER^{T2} onto the Y-chromosome.

499

500 **Animals**

501 C57BL/6J (Stock no. 000664), *Ldlr*^{KO} (Stock no. 002207), ZsGreen (Stock no. 007906), and *Myh11*-
502 CreER^{T2} (Stock no. 019079) were purchased from the Jackson Laboratory and bred in our laboratory.
503 *Adamts7* knockout mice were previously described (7). The *Cdh5*-CreER^{T2} Mouse was a gift from Dr.
504 Carol Troy (Columbia University, New York City, USA) and developed by the laboratory of Dr. Ralf Adams
505 (Max Planck Institute for Molecular Biomedicine, Münster, Germany) and has been previously described
506 (38). To generate a floxed *Adamts7*, the *Adamts7* knockout mouse (MMRRC, 046487) was bred to an
507 FLP recombinase mouse. *Adamts7* transgenic mice were created by cloning the mouse allele of *Adamts7*
508 into the pR26 CAG/GFP Asc plasmid (Addgene, plasmid # 74285). Subsequently, FL19 embryonic stem
509 cells were used to generate chimeras, which were then backcrossed to the C57BL/6J background. For
510 CreER^{T2} activation, tamoxifen (Sigma-Aldrich, T5648) was dissolved in 90% corn oil and 10% ethanol;
511 subsequently, mice at seven weeks of age were injected with tamoxifen for five days at a dosage of 40
512 mg/kg of body weight per day. At eight weeks of age, the mice were fed a WTD consisting of 40% Kcal
513 by fat and 0.15% Cholesterol (Research Diet, D12079Bi). For blood collection, mice were fasted for four
514 hours and subsequently sedated with isoflurane, and blood was collected by retroorbital puncture with
515 heparinized microcapillary tubes. Plasma was isolated by centrifugation at 1500 RCF for 10 minutes at
516 4°C. Total cholesterol was measured using the Infinity Cholesterol Reagent (Thermo Fisher Scientific,
517 TR13421).

518

519 **Atherosclerosis analysis**

520 For atherosclerosis studies, mice were sacrificed by cervical dislocation and perfused with PBS. The
521 aorta was dissected and subsequently fixed in 10% formalin. Whole aortas were stained with ORO.
522 Hearts containing the aortic root were fixed in 4% paraformaldehyde for 24 hours, transferred to 70%
523 ethanol, and embedded in paraffin wax. Sectioning was performed using a Leica microtome at 8 μm
524 thickness. The heart was sectioned from the inferior heart towards the aortic root. 25 slides were
525 collected, with each slide containing two sections. We aimed to have the breakage of the leaflet occur on
526 slide 13. Slides 3, 8,13,18, and 23 were used for hematoxylin and eosin staining to allow for lesion size
527 quantification using ImageJ. Hematoxylin and Eosin, and Picrosirius Red staining was performed at
528 Columbia's Molecular Pathology Shared Resource.
529
530 **Immunofluorescence**
531 Immunofluorescence was performed on paraffin sections of the aortic root. Deparaffinization was
532 performed using xylene. Antigen retrieval was performed using a citrate-based agent. Sections were
533 subsequently blocked using 10% normal goat serum for at least one hour. Subsequently, the sections
534 were stained using the following antibodies and dilutions 1:1000 αSMA-Cy3 (Sigma Aldrich, C6198),
535 1:500 MAC2 (Cedarlane, CL8942AP). IgG controls were purchased from Jackson Immunoresearch. The
536 sections were washed with PBS containing 0.01% Tween 20. For the secondary antibody, a donkey anti-
537 rabbit Alexa Fluor 647 (Invitrogen, A-31573) and goat anti-mouse Alexa Fluor 546 (Invitrogen, A-11030)
538 were used, both at a 1:1000 dilution in 1% goat serum. The slides were washed with DAPI and mounted
539 with ProLong Glass Antifade Mountant with NucBlue Stain. Imaging was conducted on a Nikon Eclipse
540 Ti-S microscope, and image processing was performed using ImageJ. ZsGreen fluorescence was
541 confirmed separately on unfixed frozen sections without additional antibody staining to verify reporter
542 expression.
543
544 **Vascular SMC isolation for tissue culture**

545 SMCs were isolated as previously described (39). The aorta was dissected from the ascending arch to
546 the diaphragm and was predigested for 10 minutes at 37°C with 175 U/mL Collagenase II and 1.25 U/mL
547 elastase in HBSS to allow for the removal of the adventitia. After removing the adventitia, the media layer
548 was further digested in 400 U/mL collagenase II, 2.5 U/mL elastase, and 0.2 mg/mL soybean trypsin
549 inhibitor at 37°C for one hour in a rotating incubator. The cells were cultured in DMEM supplemented
550 with 20% fetal bovine serum (FBS), 1% L-Glutamine, 1% sodium pyruvate, and 1% Penicillin
551 Streptomycin. Cells between passages two and seven were used for experiments.
552
553 **Vascular SMC isolation for flow analysis**
554 Mice were sacrificed and perfused with PBS. The ascending aorta to the bifurcation at the common iliac
555 artery was dissected and digested with a cocktail consisting of 4 U/mL Liberase TM (Sigma-Aldrich,
556 5401127001), 60 U/mL hyaluronidase (Sigma-Aldrich, H3506), and 60 U/mL DNase I (Worthington
557 Biochemical Corporation, LS006333) in RPMI-1640. The digestion enzymes were neutralized with 10%
558 FBS in RPMI and washed once in FACS buffer (2% FBS, 5 mM EDTA, 20 mM HEPES, and 1 mM Sodium
559 Pyruvate in DPBS). Cells were then blocked with TruStain FcX PLUS anti-mouse CD16/32 (Biolegend,
560 156603) for 10 mins at 4°C. Staining was performed in FACS buffer at the following dilutions: 1:1000
561 LipidTOX Red (Thermo Fisher Scientific, H34476), 1:100 CD36 Super Bright 600 (Invitrogen, 63-0362-
562 82), 1:200 CD45-Alexa Fluor 700 (Biolegend, 157209). Cell viability was assessed with DAPI. To
563 establish the LipidTOX high population and thus foamy cells, a C57BL/6J mouse with normal lipidemia
564 was used as previously described (14).
565
566 **In vitro cell culture experiments**
567 For in vitro foam cell analysis, cells were treated with DiI conjugated oxLDL (Invitrogen, L34358) at a
568 concentration of 10 µg/mL for 24 hours. Subsequently, they were washed with PBS and detached using
569 0.25% Trypsin EDTA. Neutralization of trypsin was performed using FACS buffer. The cells were
570 counterstained with DAPI to assess live cells, and all analysis was done using either a Novocyte

571 Quanteon or Penteon. For siRNA experiments, all siRNAs were purchased from Integrated DNA
572 Technologies (Supplemental Table 2). Transfection was performed using RNAiMAX according to the
573 manufacturer's protocol. All siRNAs were used at a concentration of 10 nM.
574
575 **RNA Isolation and quantitative RT-PCR**
576 For tissue samples, specimens were collected in Trizol, and homogenization was performed using a
577 tissue lyser (Qiagen). The RNA was extracted using the Direct-zol RNA MiniPrep Kit (Zymo) according
578 to the manufacturer's instructions. For cells, RNA was collected using the Quick-RNA Microprep Kit
579 (Zymo). Complementary DNA was synthesized using High-Capacity cDNA Reverse Transcription Kit
580 (Applied Biosystem). All qPCR was performed using TaqMan probes (Supplemental Table 2) and
581 performed on the Applied Biosystems QuantStudio 7 Flex Real-Time PCR System. Analysis was
582 performed using the 2-ΔΔCt Method.
583
584 **RNAscope**
585 RNAscope was performed according to the manufacturer's instructions. RNAscope was performed on
586 sections of mouse BCAs after specified durations of WTD feeding. The BCAs were freshly frozen and
587 sectioned at 8 μm thickness. The sections were first fixed in 10% neutral buffered formalin. Subsequently,
588 the sections were dehydrated and treated with hydrogen peroxide and protease. Hybridization with
589 *Adamts7* (Advanced Cell Diagnostics, 533341) and *Pecam1* (Advanced Cell Diagnostics, 316721-C3)
590 probes was performed. After probe hybridization, hybridization with AMPs 1-3 was performed. Signal
591 development was conducted using Akoya Biosciences Opal Reagent Kits, and slides were mounted
592 using Prolong Glass Antifade Mountant (Thermo Fisher Scientific, P36984). Imaging was conducted on
593 a Nikon Eclipse Ti-S microscope, and image processing was performed using ImageJ.
594
595 **Western blot**

596 Samples were lysed in RIPA buffer (Thermo Fisher Scientific, 89900) supplemented with 1% Halt
597 Protease and Phosphatase Inhibitor Cocktail. Tissue samples were lysed with the Qiagen TissueLyser
598 and samples were subsequently cleared by centrifugation at 20,000 RCF for 10 minutes at 4°C. Samples
599 were denatured, resolved on a 4-12% Bis-Tris gel, and transferred to either PVDF or a nitrocellulose
600 membrane. Blocking was performed with 5% milk, and primary antibodies were diluted 1:1000 in 5% milk
601 and incubated overnight at 4°C. The following primary antibodies were used: β-Actin (Cell Signaling
602 Technology, 5125S), Thrombospondin-1 (D7E5F) Rabbit mAb (Cell Signaling Technology, 37879S),
603 GAPDH (14C10) Rabbit mAb, HRP-conjugated (Cell Signaling Technology, 3683S), Anti-
604 COMP/Cartilage Oligomeric Matrix Protein (Abcam, ab42225), and Rabbit Ab ADAMTS7 (custom-made
605 by 21st Century Biochemicals). The custom polyclonal rabbit anti–ADAMTS7 antibody was generated
606 using standard immunization protocols with recombinant mouse ADAMTS7 as the antigen. Membranes
607 were washed with 0.1% TBST and probed with the appropriate secondary antibody for one hour at room
608 temperature. Membranes were visualized with ECL using the Amersham Imager 600 gel imager.
609
610 **RNA-seq of primary mouse vascular SMCs**
611 Primary SMCs were isolated as described above and cultured for three passages spaced one week apart.
612 Total RNA was extracted using the Zymo Microprep Kit, and RNA integrity was assessed using
613 TapeStation. No cell sorting was performed. Polyadenylated mRNA was purified from total RNA using a
614 poly(A) pull-down and reverse-transcribed into cDNA, with the final PCR step performed using KAPA HiFi
615 HotStart Ready Mix. Libraries were sequenced on the Element AVITI sequencer with 75 bp paired-end
616 reads, targeting ~40 million reads. Transcript abundance was quantified using kallisto with the GRCm38
617 mouse transcriptome, and differential expression analysis was performed using DESeq2 via DEBrowser.
618 Up and downregulated genes are listed in Supplemental Table 1.
619
620 **ATAC-seq**

621 Assay for Transposase-Accessible Chromatin using sequencing (ATAC-seq) was performed as
622 previously described with minor modifications. Briefly, 100,000 passage 3 primary mouse SMCs
623 with >90% viability were washed with PBS and pelleted at 500 × g for 5 min at 4°C. Cells were lysed in
624 cold lysis buffer (10 mM Tris-HCl pH 7.4, 10 mM NaCl, 3 mM $MgCl_2$, 0.1% NP-40, 0.1% Tween-20, and
625 0.01% digitonin). Nuclei were washed with 1 mL ATAC lysis buffer without NP-40 or digitonin and
626 centrifuged at 500 × g for 10 min at 4°C. The nuclei pellet was resuspended in transposition mix
627 containing 25 µL 2× TD buffer (Illumina Nextera DNA Library Prep Kit), 2.5 µL Tn5 transposase, 16.5 µL
628 PBS, 0.5 µL 1% digitonin, 0.5 µL 10% Tween-20, and 5 µL nuclease-free water. Transposition was carried
629 out at 37°C for 30 min in a thermomixer. DNA was purified using the Zymo DNA Clean & Concentrator-
630 5 Kit. Transposed DNA was amplified using NEBNext High-Fidelity 2× PCR Master Mix (New England
631 Biolabs, M0541) with Nextera indexing primers, and libraries were purified with AMPure XP magnetic
632 beads (Beckman Coulter, A63880). Library size distribution and quality were assessed using an Agilent
633 Bioanalyzer, and DNA concentration was measured with a Qubit dsDNA HS Assay Kit (Thermo Fisher
634 Scientific). Paired-end 150 bp sequencing was performed on an Illumina platform by Azenta/Genewiz.
635 Sequencing reads were quality-trimmed with Trimmomatic v0.38, aligned to the mm10 reference genome
636 using Bowtie2, and filtered for uniquely mapped, high-quality (MAPQ ≥30) non-duplicate reads with
637 SAMtools v1.9 and Picard v2.18.26. Reads mapping to mitochondrial DNA and unplaced contigs were
638 excluded. Peak calling was performed using MACS2 v2.1.2, with peaks overlapping ENCODE blacklisted
639 regions removed. Peaks detected in ≥66% of biological replicates per group were retained for
640 downstream analysis. Differential chromatin accessibility was determined using DiffBind (R package).
641 Sequencing yielded a total of 528 million paired-end reads (mean Q score = 36.9; 85% bases ≥ Q30).
642 After alignment (mean alignment rate = 98%) and filtering, approximately 60–100 million high-quality read
643 pairs per sample were retained for downstream analyses.
644
645 **Statistics**

646 All statistical tests are indicated in figure legends. *P* values were calculated using a 2-tailed Student's t-
647 test in GraphPad Prism 10. $P<0.05$ was considered significant. 2-way ANOVA analysis with multiple
648 corrections was used for comparison between groups with post-analysis as indicated in the figure
649 legends. Aortic root histology, qPCR, and ELISA results are presented as mean ± standard error of the
650 mean. All other data are presented as mean ± standard deviation.
651
652 **Study approval**
653 All mouse experiments were performed according to procedures approved by Columbia University's
654 Institute for Animal Care and Use Committee under protocol AABU8650. The Institutional Review Board
655 of Columbia University approved all human studies under IRB AAAJ2765 and AAAR6796 with written
656 informed consent provided by all participants.
657
658 **Data availability**
659 Human carotid artery scRNA-seq has been previously published (19). ATAC and RNA-seq data have
660 been deposited in the NCBI's Gene Expression Omnibus database (GSE316135). All individual values
661 represented in graphs are provided in the Supporting Data Values file.
662
663 **AUTHOR CONTRIBUTIONS**
664 A.C. led the study and directly performed the majority of experiments. H.K.C., K.S., C.V.M., and J.G. P.
665 conducted experiments and acquired data. H.P. contributed to the generation of mouse lines. L.E.F. and
666 J.S.K. performed ATAC-seq data analysis. A.C.B., H.Y., and M.L. provided human single-cell datasets.
667 R.C.B. oversaw study design, execution, management, and funding. A.C. and R.C.B. wrote the
668 manuscript, with all authors reviewing and approving the final version.
669
670 **FUNDING SUPPORT**

671 This work is the result of NIH funding, in whole or in part, and is subject to the NIH Public Access Policy.
672 Through acceptance of this federal funding, the NIH has been given a right to make the work publicly
673 available in PubMed Central. A.C. is supported by an American Heart Association Predoctoral Fellowship
674 909206 and the NIH Graduate Training in Nutrition grant 5T32DK007647. L.E.F. is supported by NIH
675 grant 5T32DK007647. H.P. is supported by NIH grants 5K99HL153939 and R00HL153939. A.C.B. is
676 supported by the NIH Postdoctoral Training in Arteriosclerosis Fellowship 5T32HL007343. K.S. is
677 supported by NIH Training in Cellular, Molecular, and Biomedical Studies 5T32GM145766. M.L. is
678 supported by NIH grants R01GM125301, R01HL113147, R01HL150359, and R21HL156234. R.C.B. is
679 supported for this work by NIH grants R01HL141745 and R01DK134026.

680

681 **ACKNOWLEDGMENTS**

682 We thank Dr. Muredach P. Reilly for guidance in the execution of these studies and Dr. Elizabeth E. Ha
683 for helpful discussions. We acknowledge the staff of the Columbia Stem Cell Initiative Flow Cytometry
684 Core Facility, led by Michael Kissner at Columbia University Irving Medical Center, for their technical
685 support. We also thank Dr. Carol Troy for generously providing the *Cdh5*-CreER^{T2} mice.

686

687 **REFERENCE**

688 1. Tsao CW, Aday AW, Almarzooq ZI, Anderson CAM, Arora P, Avery CL, et al. Heart Disease
689 and Stroke Statistics-2023 Update: A Report From the American Heart Association. *Circulation.*
690 2023.
691 2. Aragam KG, Jiang T, Goel A, Kanoni S, Wolford BN, Atri DS, et al. Discovery and systematic
692 characterization of risk variants and genes for coronary artery disease in over a million
693 participants. *Nat Genet.* 2022;54(12):1803-15.
694 3. Nikpay M, Goel A, Won HH, Hall LM, Willenborg C, Kanoni S, et al. A comprehensive 1,000
695 Genomes-based genome-wide association meta-analysis of coronary artery disease. *Nat*
696 *Genet.* 2015;47(10):1121-30.

697 4. Reilly MP, Li M, He J, Ferguson JF, Stylianou IM, Mehta NN, et al. Identification of ADAMTS7
698 as a novel locus for coronary atherosclerosis and association of ABO with myocardial infarction
699 in the presence of coronary atherosclerosis: two genome-wide association studies. *Lancet.*
700 2011;377(9763):383-92.
701 5. Schunkert H, Konig IR, Kathiresan S, Reilly MP, Assimes TL, Holm H, et al. Large-scale
702 association analysis identifies 13 new susceptibility loci for coronary artery disease. *Nat Genet.*
703 2011;43(4):333-8.
704 6. Luan Y, Kong L, Howell DR, Ilalov K, Fajardo M, Bai XH, et al. Inhibition of ADAMTS-7 and
705 ADAMTS-12 degradation of cartilage oligomeric matrix protein by alpha-2-macroglobulin.
706 *Osteoarthritis Cartilage.* 2008;16(11):1413-20.
707 7. Bauer RC, Tohyama J, Cui J, Cheng L, Yang J, Zhang X, et al. Knockout of Adamts7, a novel
708 coronary artery disease locus in humans, reduces atherosclerosis in mice. *Circulation.*
709 2015;131(13):1202-13.
710 8. Chung A, Reilly MP, and Bauer RC. ADAMTS7: a Novel Therapeutic Target in Atherosclerosis.
711 *Curr Atheroscler Rep.* 2023;25(8):447-55.
712 9. Mizoguchi T, MacDonald BT, Bhandary B, Popp NR, Laprise D, Arduini A, et al. Coronary
713 Disease Association With ADAMTS7 Is Due to Protease Activity. *Circ Res.* 2021;129(4):458-70.
714 10. Ma Z, Mao C, Chen X, Yang S, Qiu Z, Yu B, et al. Peptide Vaccine Against ADAMTS-7
715 Ameliorates Atherosclerosis and Postinjury Neointima Hyperplasia. *Circulation.* 2022.
716 11. Miano JM, Fisher EA, and Majesky MW. Fate and State of Vascular Smooth Muscle Cells in
717 Atherosclerosis. *Circulation.* 2021;143(21):2110-6.
718 12. Pan H, Xue C, Auerbach BJ, Fan J, Bashore AC, Cui J, et al. Single-Cell Genomics Reveals a
719 Novel Cell State During Smooth Muscle Cell Phenotypic Switching and Potential Therapeutic
720 Targets for Atherosclerosis in Mouse and Human. *Circulation.* 2020;142(21):2060-75.

721 13. Shankman LS, Gomez D, Cherepanova OA, Salmon M, Alencar GF, Haskins RM, et al. KLF4-
722 dependent phenotypic modulation of smooth muscle cells has a key role in atherosclerotic
723 plaque pathogenesis. *Nat Med.* 2015;21(6):628-37.
724 14. Wang Y, Dubland JA, Allahverdian S, Asonye E, Sahin B, Jaw JE, et al. Smooth Muscle Cells
725 Contribute the Majority of Foam Cells in ApoE (Apolipoprotein E)-Deficient Mouse
726 Atherosclerosis. *Arterioscler Thromb Vasc Biol.* 2019;39(5):876-87.
727 15. Wang L, Zheng J, Bai X, Liu B, Liu CJ, Xu Q, et al. ADAMTS-7 mediates vascular smooth
728 muscle cell migration and neointima formation in balloon-injured rat arteries. *Circ Res.*
729 2009;104(5):688-98.
730 16. Santamaria S, and de Groot R. ADAMTS proteases in cardiovascular physiology and disease.
731 *Open Biol.* 2020;10(12):200333.
732 17. Kessler T, Zhang L, Liu Z, Yin X, Huang Y, Wang Y, et al. ADAMTS-7 inhibits re-
733 endothelialization of injured arteries and promotes vascular remodeling through cleavage of
734 thrombospondin-1. *Circulation.* 2015;131(13):1191-201.
735 18. Zhang Y, Lin J, and Wei F. The Function and Roles of ADAMTS-7 in Inflammatory Diseases.
736 *Mediators Inflamm.* 2015;2015:801546.
737 19. Bashore AC, Yan H, Xue C, Zhu LY, Kim E, Mawson T, et al. High-Dimensional Single-Cell
738 Multimodal Landscape of Human Carotid Atherosclerosis. *Arterioscler Thromb Vasc Biol.*
739 2024;44(4):930-45.
740 20. Allahverdian S, Chaabane C, Boukais K, Francis GA, and Bochaton-Piallat ML. Smooth muscle
741 cell fate and plasticity in atherosclerosis. *Cardiovasc Res.* 2018;114(4):540-50.
742 21. Bashore AC, Chung A, Ibikunle C, Yan H, Xue C, Li M, et al. Single-Cell Multimodal Profiling of
743 Atherosclerosis Identifies CD200 as a Cell Surface Lineage Marker of Vascular Smooth Muscle
744 Cells and Their Derived Cells. *Circulation.* 2024;149(15):1231-3.

745 22. Poznyak AV, Nikiforov NG, Markin AM, Kashirskikh DA, Myasoedova VA, Gerasimova EV, et al.
746 Overview of OxLDL and Its Impact on Cardiovascular Health: Focus on Atherosclerosis. *Front*
747 *Pharmacol.* 2020;11:613780.
748 23. Chattopadhyay A, Kwartler CS, Kaw K, Li Y, Kaw A, Chen J, et al. Cholesterol-Induced
749 Phenotypic Modulation of Smooth Muscle Cells to Macrophage/Fibroblast-like Cells Is Driven by
750 an Unfolded Protein Response. *Arterioscler Thromb Vasc Biol.* 2021;41(1):302-16.
751 24. Jay AG, Chen AN, Paz MA, Hung JP, and Hamilton JA. CD36 binds oxidized low density
752 lipoprotein (LDL) in a mechanism dependent upon fatty acid binding. *J Biol Chem.*
753 2015;290(8):4590-603.
754 25. Karin M. The regulation of AP-1 activity by mitogen-activated protein kinases. *J Biol Chem.*
755 1995;270(28):16483-6.
756 26. Tcheandjieu C, Zhu X, Hilliard AT, Clarke SL, Napolioni V, Ma S, et al. Large-scale genome-
757 wide association study of coronary artery disease in genetically diverse populations. *Nat Med.*
758 2022;28(8):1679-92.
759 27. Pu X, Xiao Q, Kiechl S, Chan K, Ng FL, Gor S, et al. ADAMTS7 cleavage and vascular smooth
760 muscle cell migration is affected by a coronary-artery-disease-associated variant. *Am J Hum*
761 *Genet.* 2013;92(3):366-74.
762 28. Kan H, Zhang K, Mao A, Geng L, Gao M, Feng L, et al. Single-cell transcriptome analysis
763 reveals cellular heterogeneity in the ascending aortas of normal and high-fat diet-fed mice. *Exp*
764 *Mol Med.* 2021;53(9):1379-89.
765 29. Sharma D, Worssam MD, Pedroza AJ, Dalal AR, Alemany H, Kim HJ, et al. Comprehensive
766 Integration of Multiple Single-Cell Transcriptomic Data Sets Defines Distinct Cell Populations
767 and Their Phenotypic Changes in Murine Atherosclerosis. *Arterioscler Thromb Vasc Biol.*
768 2024;44(2):391-408.
769 30. Dubland JA, Allahverdian S, Besler KJ, Ortega C, Wang Y, Pryma CS, et al. Low LAL
770 (Lysosomal Acid Lipase) Expression by Smooth Muscle Cells Relative to Macrophages as a

771 Mechanism for Arterial Foam Cell Formation. *Arterioscler Thromb Vasc Biol.* 2021;41(6):e354-
772 e68.
773 31. Miller CL, and Zhang H. Clarifying the Distinct Roles of Smooth Muscle Cell-Derived Versus
774 Macrophage Foam Cells and the Implications in Atherosclerosis. *Arterioscler Thromb Vasc Biol.*
775 2021;41(6):2035-7.
776 32. Kim K, Shim D, Lee JS, Zaitsev K, Williams JW, Kim KW, et al. Transcriptome Analysis Reveals
777 Nonfoamy Rather Than Foamy Plaque Macrophages Are Proinflammatory in Atherosclerotic
778 Murine Models. *Circ Res.* 2018;123(10):1127-42.
779 33. Sharifi MA, Wierer M, Dang TA, Milic J, Moggio A, Sachs N, et al. ADAMTS-7 Modulates
780 Atherosclerotic Plaque Formation by Degradation of TIMP-1. *Circ Res.* 2023;133(8):674-86.
781 34. Inaba T, Gotoda T, Ishibashi S, Harada K, Ohsuga JI, Ohashi K, et al. Transcription factor PU.1
782 mediates induction of c-fms in vascular smooth muscle cells: a mechanism for phenotypic
783 change to phagocytic cells. *Mol Cell Biol.* 1996;16(5):2264-73.
784 35. MacDonald BT, Keshishian H, Mundorff CC, Arduini A, Lai D, Bendinelli K, et al. TAILS
785 Identifies Candidate Substrates and Biomarkers of ADAMTS7, a Therapeutic Protease Target in
786 Coronary Artery Disease. *Mol Cell Proteomics.* 2022;21(4):100223.
787 36. Colige A, Monseur C, Crawley JTB, Santamaria S, and de Groot R. Proteomic discovery of
788 substrates of the cardiovascular protease ADAMTS7. *J Biol Chem.* 2019;294(20):8037-45.
789 37. Liu CJ, Kong W, Ilalov K, Yu S, Xu K, Prazak L, et al. ADAMTS-7: a metalloproteinase that
790 directly binds to and degrades cartilage oligomeric matrix protein. *FASEB J.* 2006;20(7):988-90.
791 38. Sorensen I, Adams RH, and Gossler A. DLL1-mediated Notch activation regulates endothelial
792 identity in mouse fetal arteries. *Blood.* 2009;113(22):5680-8.
793 39. Ostriker AC, Xie Y, Chakraborty R, Sizer AJ, Bai Y, Ding M, et al. TET2 Protects Against
794 Vascular Smooth Muscle Cell Apoptosis and Intimal Thickening in Transplant Vasculopathy.
795 *Circulation.* 2021;144(6):455-70.
796

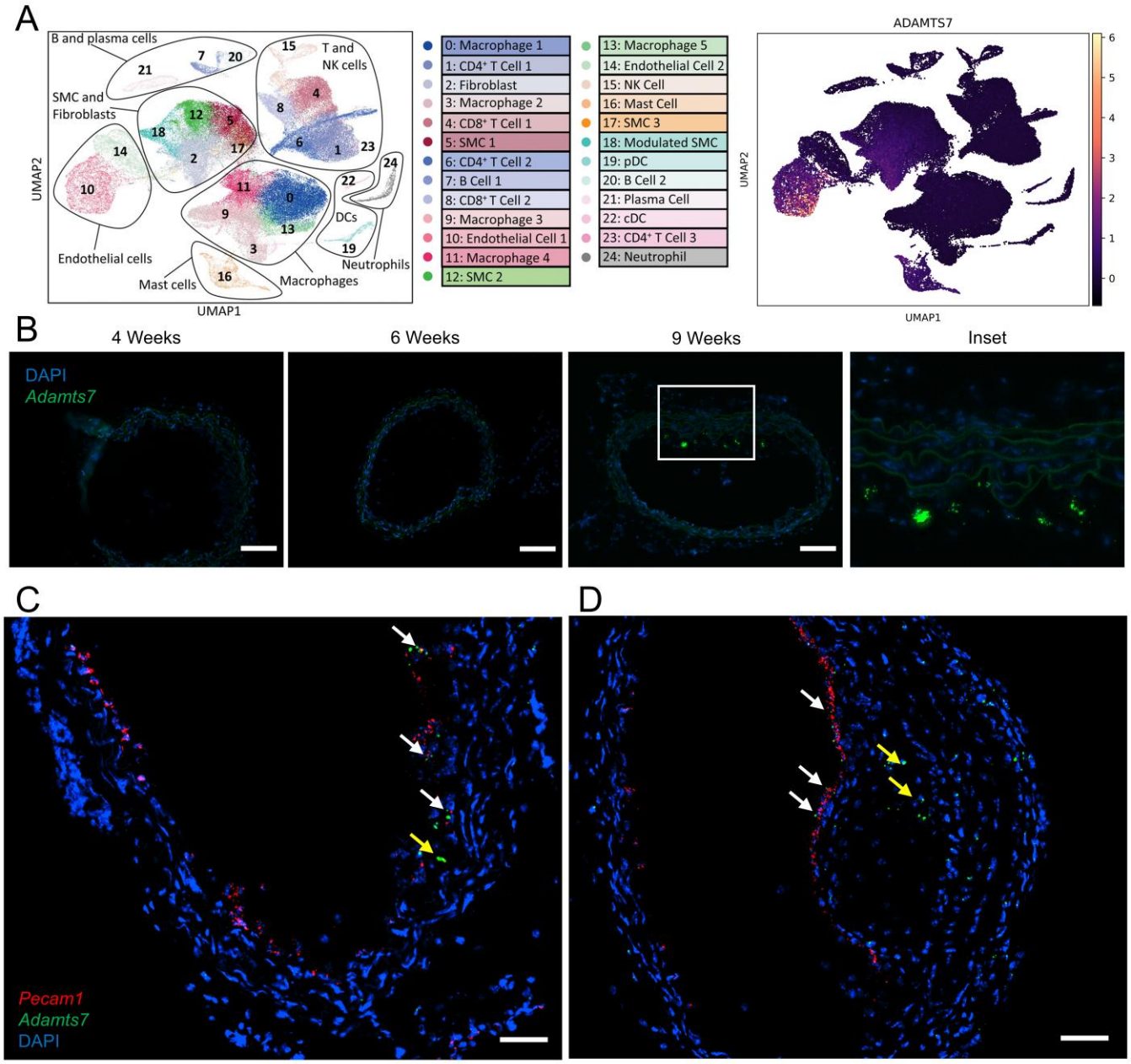
A
B and plasma cells
T and NK cells
SMC and Fibroblasts
Endothelial cells
Mast cells
Macrophages
DCs
Neutrophils
UMAP1
UMAP2
0: Macrophage 1
1: CD4⁺ T Cell 1
2: Fibroblast
3: Macrophage 2
4: CD8⁺ T Cell 1
5: SMC 1
6: CD4⁺ T Cell 2
7: B Cell 1
8: CD8⁺ T Cell 2
9: Macrophage 3
10: Endothelial Cell 1
11: Macrophage 4
12: SMC 2
13: Macrophage 5
14: Endothelial Cell 2
15: NK Cell
16: Mast Cell
17: SMC 3
18: Modulated SMC
19: pDC
20: B Cell 2
21: Plasma Cell
22: cDC
23: CD4⁺ T Cell 3
24: Neutrophil
ADAMTS7
B
4 Weeks
6 Weeks
9 Weeks
Inset
DAPI
Adamts7
C
D
Pecam1
Adamts7
DAPI

804 **Figure 1. Identifying endogenous ADAMTS7 expression.** (A) Single Cell RNA sequencing of human
805 carotid atherosclerosis and cell clustering identities. Cluster identities are reproduced with permission
806 from Bashore AC et al., Arterioscler Thromb Vasc Biol. 2024;44:930–945. (B) RNAscope of the BCA in
807 mice after WTD feeding. Nuclei are stained with DAPI. Scale bar = 100 μm. RNAscope of the BCA of
808 *Ldlr*^{KO} mice after seven (C) and ten (D) weeks of WTD feeding and probed against *Adamts7* and *Pecam1*.
809 White arrows highlight EC expression of *Adamts7*. Yellow arrows indicate non-EC expression of
810 *Adamts7*. Scale bar = 50 μm.

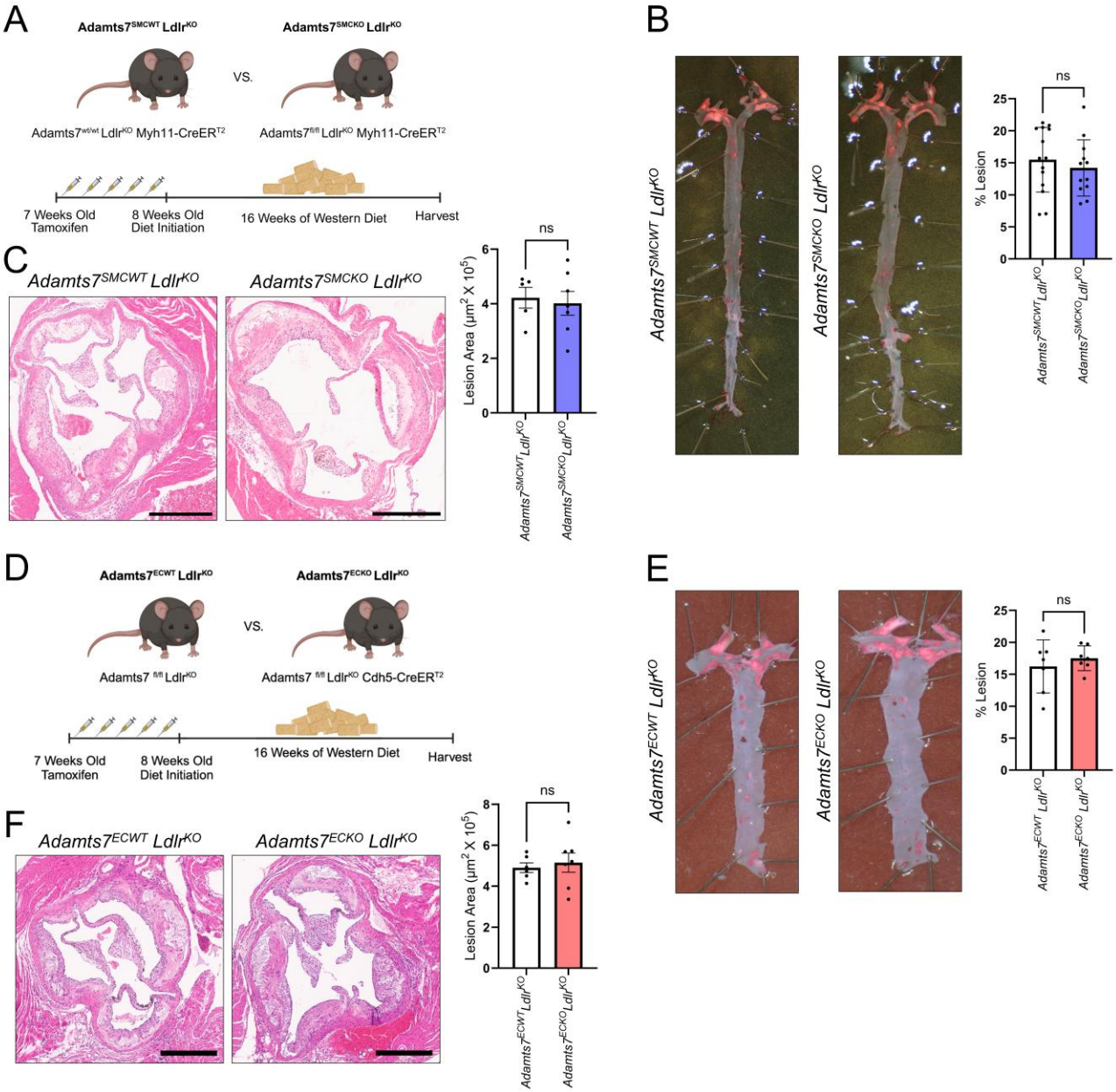

811

812

813

814

815

816

817 **Figure 2. SMC or EC knockout of *Adamts7* does not affect atherosclerosis.** (A) Schematic outlining
818 experimental design and mouse comparisons for SMC knockout of *Adamts7*. Created with
819 BioRender.com (B) Representative ORO staining of en face aortas and enumeration. *n* = 12 - 14. (C)
820 Representative images of hematoxylin and eosin (H&E) stained aortic root sections, quantification of
821 plaque areas *n* = 5 - 7. Scale bar = 500 μm. (D) Schematic outlining experimental design and mouse
822 comparisons for EC knockout of *Adamts7*. Created with BioRender.com (E) Representative ORO staining
823 of en face aortas and enumeration. *n* = 7. (F) Representative images of H&E stained aortic root sections,
824 quantification of plaque areas *n* = 6 - 7. Scale bar = 500 μm. Statistics were analyzed using a 2-tailed
825 Student's t-test.

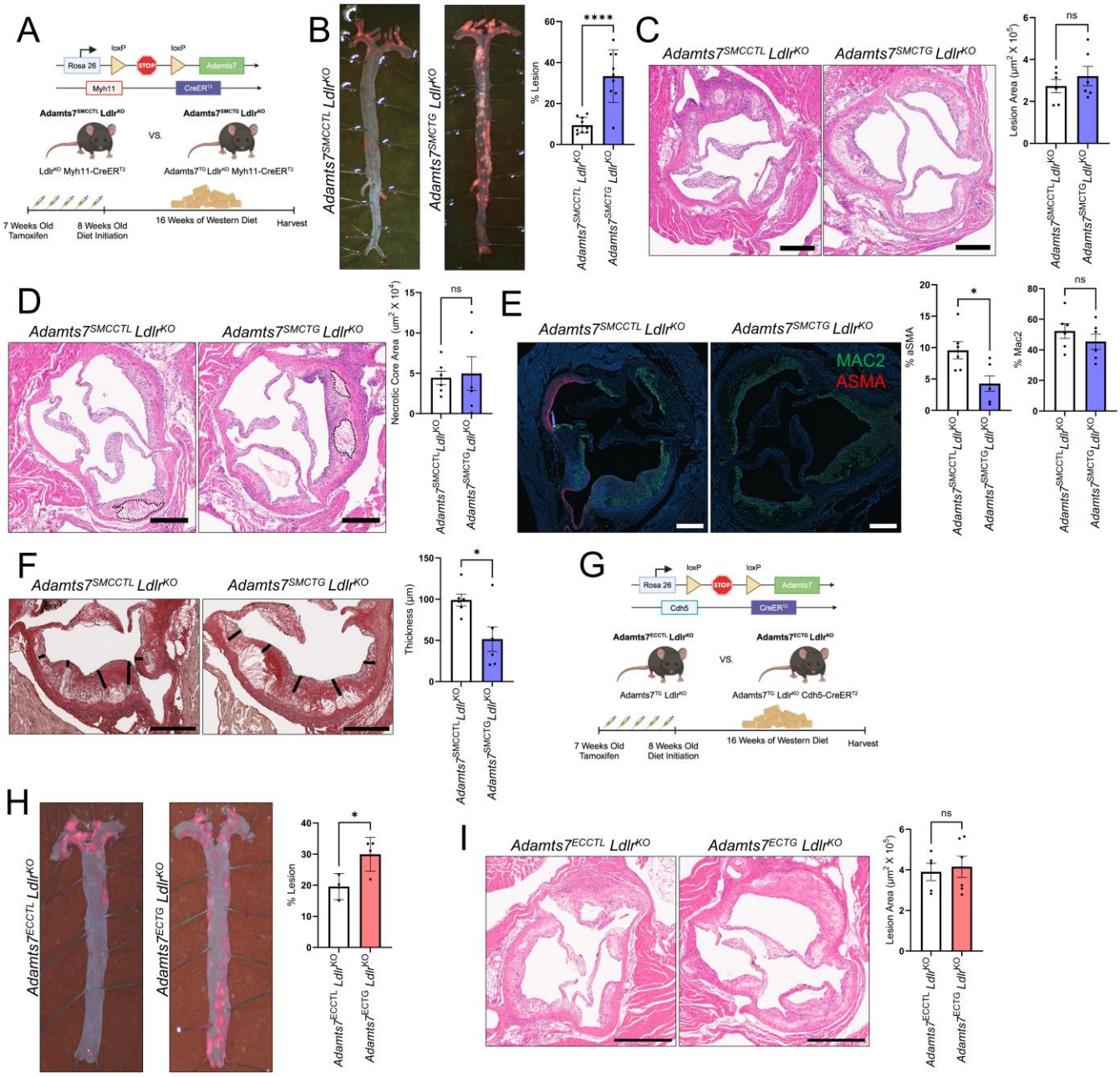

826

827

828

829

830

831

832 **Figure 3. SMC and EC transgenic *Adamts7* increases aortic atherosclerosis.** (A) Schematic
833 outlining experimental design and the generation of the SMC transgenic ADAMTS7 mouse. Created with
834 BioRender.com (B) ORO staining of the en face aorta and quantification of lesion area. n = 9. (C)
835 Representative images of H&E stained aortic root sections, quantification of plaque areas n = 6. Scale
836 bar = 500 μm. (D) Representative images of H&E stained aortic root sections with necrotic core outlined
837 in dotted line n = 6 mice. Scale bar = 300 μm. (E) Representative images of aortic root sections stained
838 against α-SMA (Cy3 - red), MAC2 (Alexa Fluor 488 - green), and cell nuclei (DAPI - blue) with their
839 subsequent quantification relative to lesion area n = 6. Scale bar = 300 μm. (F) Representative picrosirius
840 red staining of aortic root lesions with bars indicating fibrous cap thickness and quantification of fibrous
841 cap thickness n = 6. Scale bar = 300 μm. (G) Schematic outlining experimental design and the generation
842 of the EC transgenic ADAMTS7 mouse. Created with BioRender.com (H) ORO staining of the en face
843 aorta and quantification of lesion area. n = 3 - 4. (I) Representative images of H&E stained aortic root
844 sections, quantification of plaque areas n = 5 - 6. Scale bar = 500 μm. ****P<0.0001, ***P<0.001, **
845 P<0.01, *P<0.05. Statistics were analyzed using a 2-tailed Student's t-test.

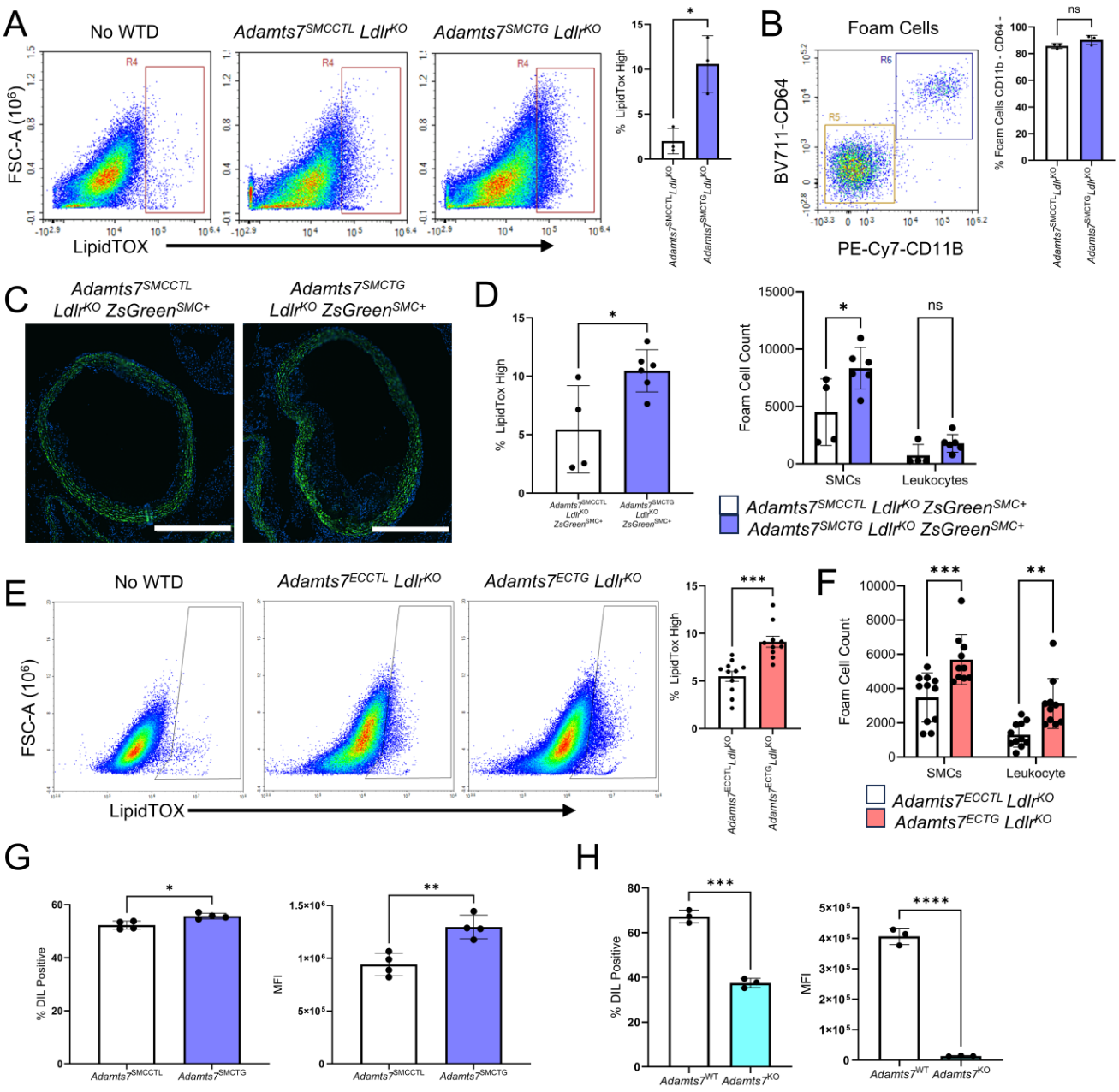
A
No WTD
Adamts7SMCCTL LdlrKO
Adamts7SMCTG LdlrKO
FSC-A (10^6)
LipidTOX
% LipidTox High
B
Foam Cells
BV711-CD64
PE-Cy7-CD11B
% Foam Cells CD11b - CD64 -
ns
C
Adamts7SMCCTL LdlrKO ZsGreenSMC+
Adamts7SMCTG LdlrKO ZsGreenSMC+
D
% LipidTox High
Foam Cell Count
SMCs
Leukocytes
Adamts7SMCCTL LdlrKO ZsGreenSMC+
Adamts7SMCTG LdlrKO ZsGreenSMC+
E
No WTD
Adamts7ECCTL LdlrKO
Adamts7ECTG LdlrKO
FSC-A (10^6)
LipidTOX
% LipidTox High
F
Foam Cell Count
SMCs
Leukocyte
Adamts7ECCTL LdlrKO
Adamts7ECTG LdlrKO
G
% DIL Positive
MFI
H
% DIL Positive
MFI

852 **Figure 4. ADAMTS7 promotes foam cell expansion.** (A) Flow cytometry-based quantification of foam
853 cells through LipidTOX staining of the aorta. A normolipidemic aorta was used to establish the LipidTOX
854 high gate. *n* = 3 (B) Breakdown of foam cells stained positively for CD11B and CD64 *n* = 3. (C)
855 Confirmation of efficient ZsGreen labeling of SMCs with nuclei counterstained with DAPI. Scale bar =
856 500 μm. (D) Foam cell analysis with the SMC lineage tracer ZsGreen and leukocyte marker CD45 after
857 12 weeks of WTD. Counts were normalized to 100,000 live cells. *n* = 4 - 6 mice. Statistics were analyzed
858 by two-way ANOVA with Sidak's multiple comparison test. (E) Flow cytometry-based quantification of
859 foam cells through LipidTOX staining of the aorta. A normolipidemic aorta was used to establish the
860 LipidTOX high gate. *n* = 3 - 4. (F) Normalized foam cell counts out of 100,000 live cells after 16 weeks of
861 WTD. Leukocytes were identified as $CD45^{+}$. SMCs were identified as $CD31^{-}$ $CD45^{-}$ $CD200^{+}$. *n* = 10 - 11
862 mice. Statistics were analyzed by two-way ANOVA with Sidak's multiple comparison test. (G) In vitro
863 foam cell analysis with primary cells from transgenic mice treated with 10 μg/mL DiI-oxLDL for 24 hours,
864 *n* = 4. (H) In vitro foam cell analysis with explanted primary SMCs from whole body *Adamts7* knockout
865 mice treated with 10 μg/mL DiI-oxLDL for 24 hours, *n* = 3. ****$P<0.0001$, ***$P<0.001$, ** $P<0.01$, *$P<0.05$
866 Between sample comparisons were analyzed by a 2-tailed Student's t-test.

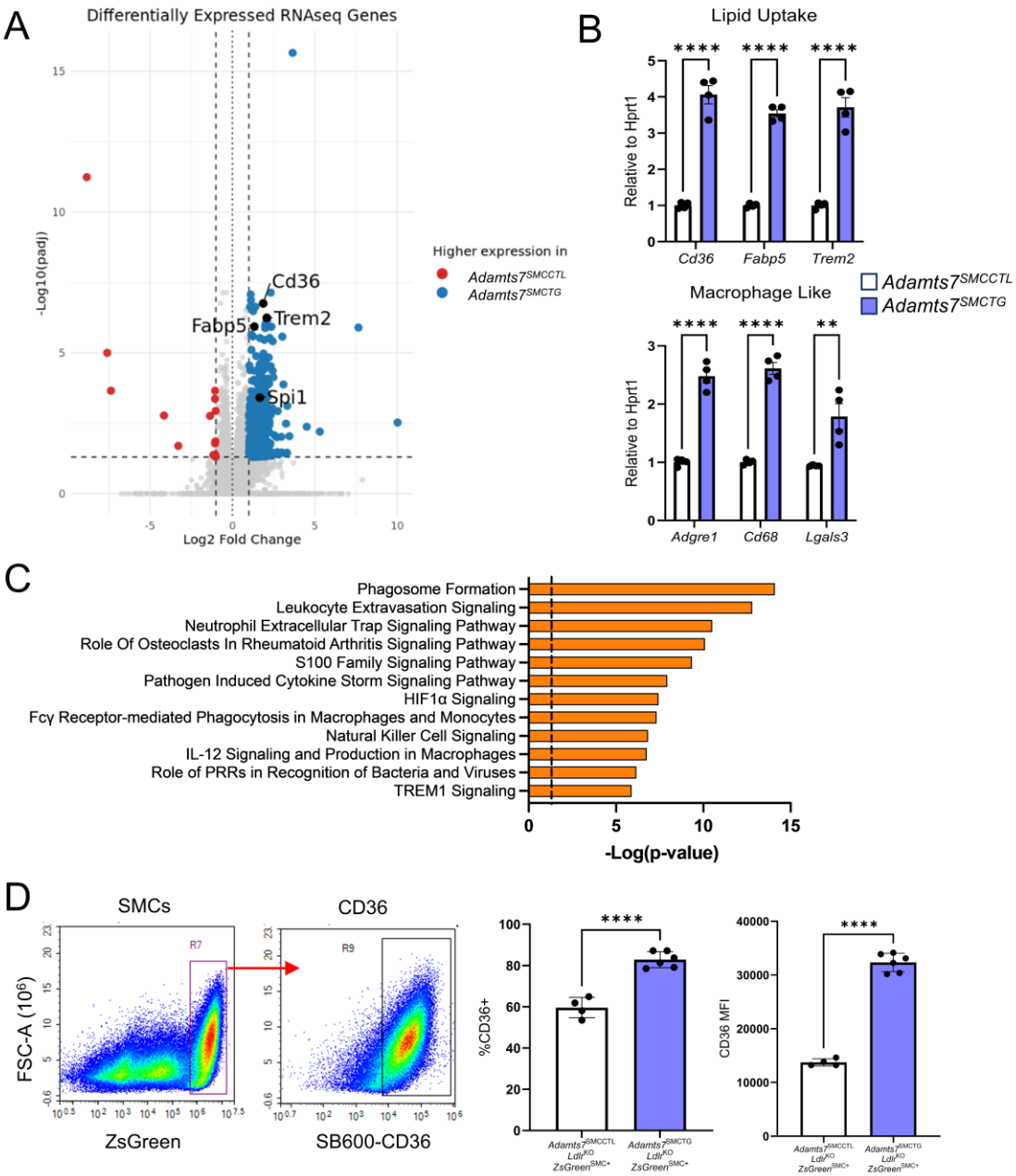

867

868

869

870

871

872

873 **Figure 5. Bulk RNA-seq of *Adamts7*^{SMCTG} primary SMCs reveals an increase in lipid handling**
874 **genes.** (A) Volcano plot of the most upregulated and downregulated genes by *P* value adjusted for
875 multiple comparisons. Passage two cells were used for RNA-seq. *Adamts7* (x = 3.65, y = 122) was
876 excluded from the plot for visualization purposes because it fell completely off scale. (B) qRT-PCR
877 confirmation of upregulated lipid uptake and macrophage-like genes $n = 4$. Normalization was performed
878 relative to *Hprt1*. (C) Ingenuity Pathway Analysis of differentially expressed genes with Ingenuity
879 Canonical Pathways highlighted. Shown pathways are predicted to be upregulated within *Adamts7*^{SMCTG}
880 primary SMCs. (D) Confirmation of enhanced SMC CD36 in vivo. Flow cytometry analysis of lineage
881 traced mice after 12 weeks of WTD feeding $n = 4 - 6$ mice. ****$P<0.0001$, **$P<0.01$ Statistics were
882 analyzed using a 2-tailed Student's t-test.

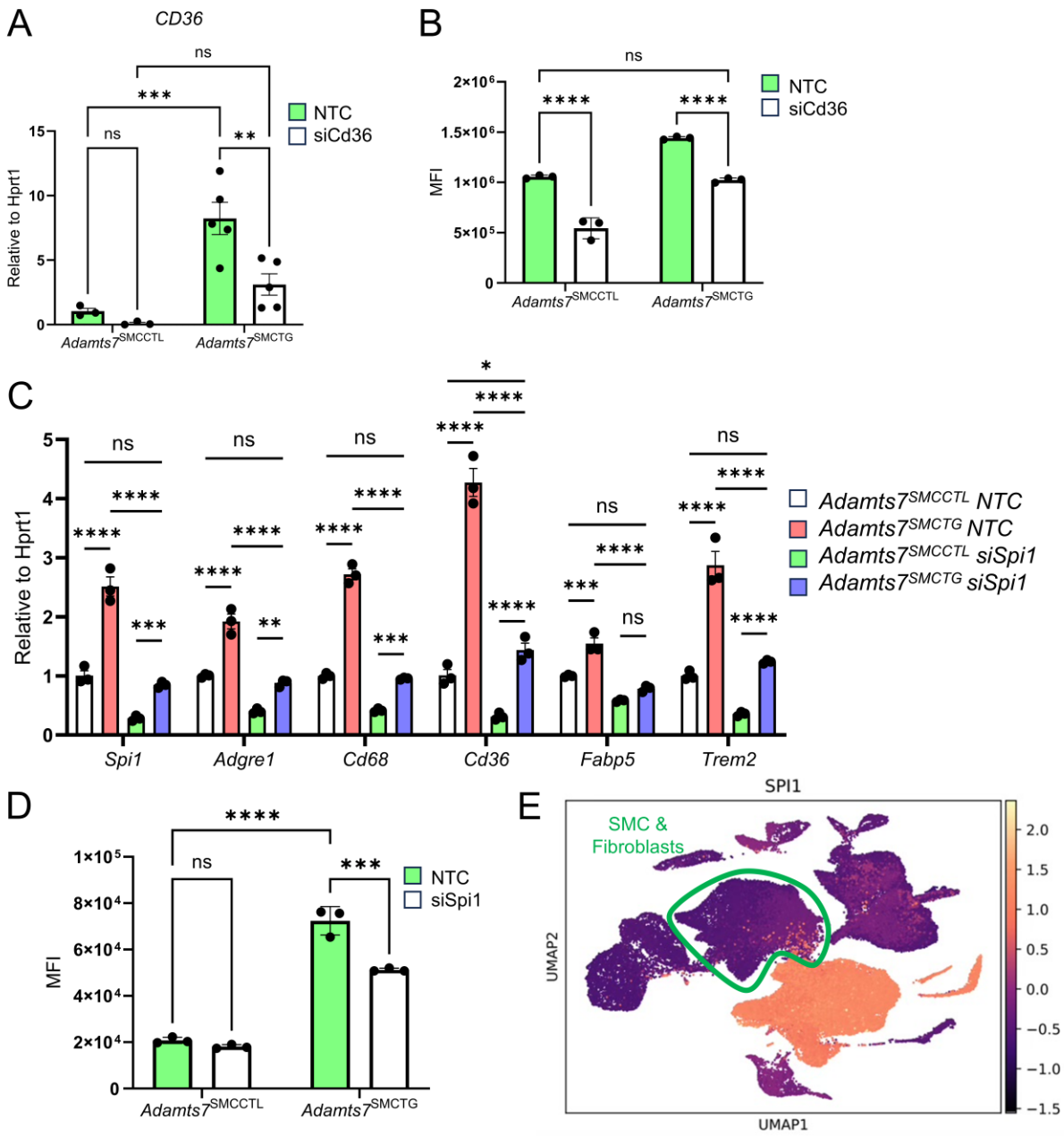

883

884

885

886

887

888

889 **Figure 6. CD36 and PU.1 mediate ADAMTS7 conferred foam cell expansion.** (A) Confirmation of
890 knockdown of *Cd36* through siRNA. Primary SMCs were treated with 10 nM of either an NTC or *Cd36*
891 siRNA. Knockdown was assessed 48 hours after transfection n = 3 - 5 mice. (B) Flow analysis of oxLDL
892 lipid uptake. 24 hours post siRNA transfection, cells were treated with 10 µg/mL of DiI-oxLDL, and uptake
893 was assessed 24 hours post oxLDL treatment n = 3. (C) Knockdown of *Spi1* in primary SMCs. Cells were
894 treated with 10 nM of siRNA, and 48 hours after transfection, cells were harvested for qRT-PCR. (D) Flow
895 analysis of lipid uptake. 24 hours post *Spi1* siRNA transfection, cells were treated with 10ug/mL of DiI-
896 oxLDL, and uptake was assessed 24 hours post oxLDL treatment. (E) Expression of *SPI1* in human
897 carotid atherosclerosis. ****P<0.0001, ***P<0.001, ** P<0.01, *P<0.05 Statistics were analyzed by two-
898 way ANOVA with Sidak's multiple comparison test.

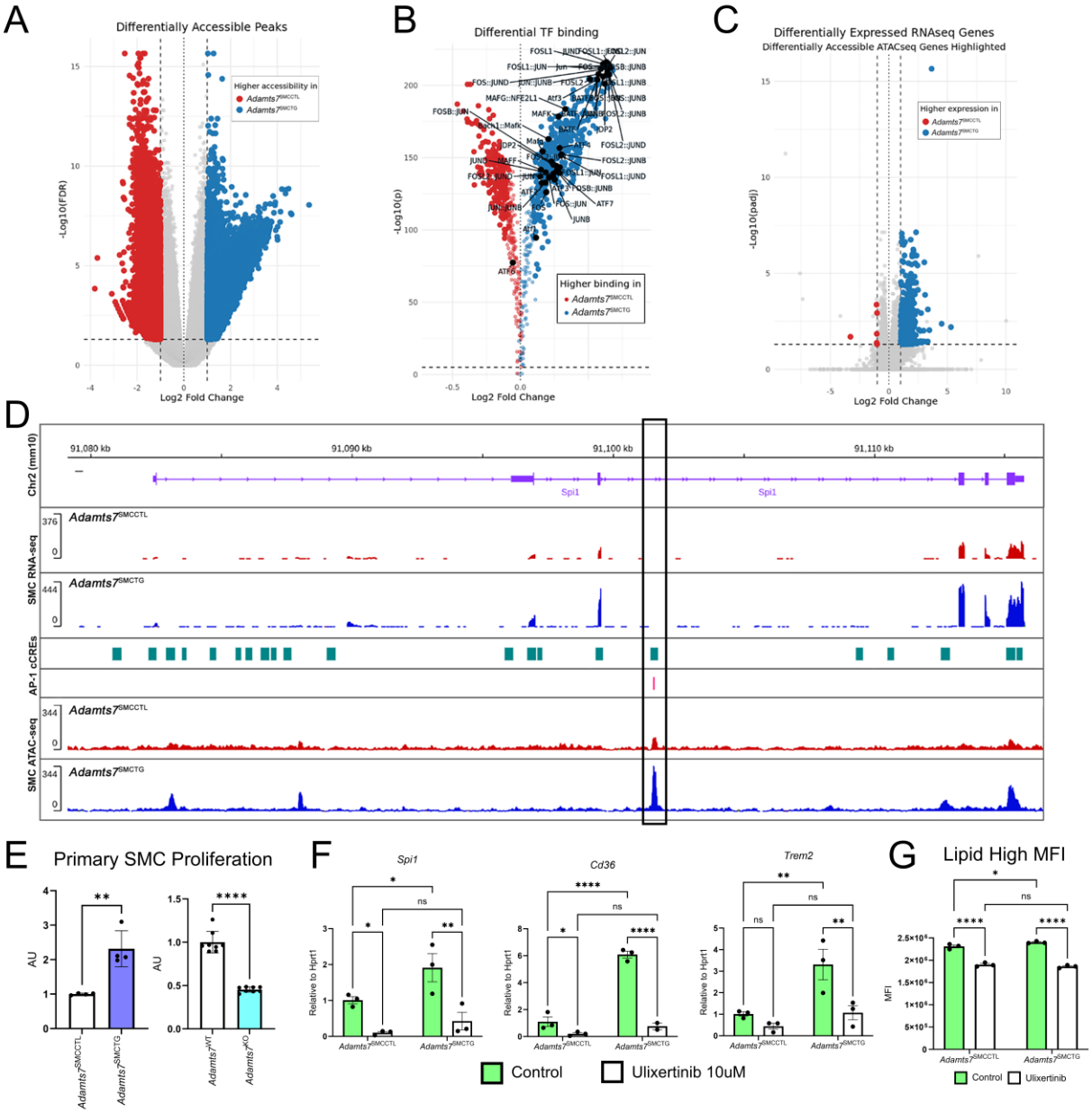
A
Differentially Accessible Peaks
Higher accessibility in
Adamts7SMCCTL
Adamts7SMCTG
-Log10(FDR)
Log2 Fold Change
B
Differential TF binding
Higher binding in
Adamts7SMCCTL
Adamts7SMCTG
-Log10(p)
Log2 Fold Change
C
Differentially Expressed RNAseq Genes
Differentially Accessible ATACseq Genes Highlighted
Higher expression in
Adamts7SMCCTL
Adamts7SMCTG
-Log10(padj)
Log2 Fold Change
D
Chr2 (mm10)
91,080 kb
91,090 kb
91,100 kb
91,110 kb
Spi1
Spi1
SMC RNA-seq
Adamts7SMCCTL
Adamts7SMCTG
AP-1 cCREs
SMC ATAC-seq
Adamts7SMCCTL
Adamts7SMCTG
E
Primary SMC Proliferation
AU
Adamts7SMCCTL
Adamts7SMCTG
Adamts7WT
Adamts7KO
F
Spi1
Cd36
Trem2
Relative to Hprt1
Adamts7SMCCTL
Adamts7SMCTG
Control
Ulixertinib 10uM
G
Lipid High MFI
MFI
Adamts7SMCCTL
Adamts7SMCTG
Control
Ulixertinib

905 **Figure 7. ADAMTS7 drives AP-1–dependent chromatin remodeling and transcriptional**
906 **reprogramming in SMCs.** (A) Differential ATAC-seq peaks in primary SMCs from *Adamts7*^{SMCCTL} and
907 *Adamts7*^{SMCTG} mice reveal widespread chromatin remodeling. (B) Motif enrichment analysis of differential
908 peaks identifies significant overrepresentation of FOS and JUN (AP-1) binding sites. (C) Integration of
909 ATAC-seq and RNA-seq data shows that 85.8% of genes upregulated in *Adamts7*^{SMCTG} SMCs are
910 associated with nearby differential ATAC peaks (±100 kb from TSS). (D) Genome browser tracks at the
911 *Spi1* locus indicate increased chromatin accessibility in *Adamts7*^{SMCTG} SMCs at a predicted cis-regulatory
912 element containing an AP-1 motif. (E) Proliferation as determined by CellTiter of primary SMCs of
913 *Adamts7* overexpression $n = 4$ and *Adamts7* knockout cells $n = 8$. (F) qRT-PCR of ERK1/2 inhibition with
914 Ulixertinib suppresses ADAMTS7-induced upregulation of *Spi1*, lipid-handling genes (*Cd36*, *Trem2*). (G)
915 Ulixertinib treatment and subsequent DiI-oxLDL uptake in primary SMCs $n = 3$. Statistics were analyzed
916 using a 2-tailed Student's t-test or two-way ANOVA with Sidak's multiple comparison test. ****$P<0.0001$,
917 ***$P<0.001$, **$P<0.01$, *$P<0.05$
918
919
920
921
922
923
924
925
926
927
928
929

Upstream Regulator	Expr Fold Change	Molecule Type	Activation z-score
lipopolysaccharide	-	chemical drug	5.491
TNF	-	cytokine	5.103
E. coli B4 lipopolysaccharide	-	chemical toxicant	4.872
tetradecanoylphorbol acetate	-	chemical drug	4.833
SPI1	**3.16**	**transcription regulator**	**4.682**
CSF2	-	cytokine	4.675
AGT	-	growth factor	4.593
OGA	-	enzyme	4.593
tretinoin	-	chemical drug	4.484
CNTF	-	cytokine	4.243
cardiotoxin	-	chemical - other	4.123
BHLHE40	**-**	**transcription regulator**	**4.022**
IL33	-	cytokine	3.943
SMARCA4	**-**	**transcription regulator**	**3.939**
CEBPA	**3.969**	**transcription regulator**	**3.913**
D-glucose	-	chemical - endogenous mammalian	3.907
USP22	-	peptidase	3.898
CD44	-	other	3.843
poly rI:rC-RNA	-	biologic drug	3.814
IFNG	-	cytokine	3.703
ITPR2	-	ion channel	3.592
TGM2	-	enzyme	3.568
bleomycin	-	biologic drug	3.567
KLF6	**-**	**transcription regulator**	**3.549**
dihydrotestosterone	-	chemical - endogenous mammalian	3.539

930

931 **Table 1. IPA upstream regulator analysis to identify candidate TFs**. Upstream regulator analysis of
932 RNA-seq reveals activated candidate molecules responsible for the gene expression changes. Five TFs
933 are listed within the top 25 listed molecules.